

# 1 **Electrolytic-Dielectrics: A route to zero recast Electrical Discharge Machining**

2

## 3 **Abstract**

4

5 Electrical discharge machining (EDM) is a widely used manufacturing process for machining hard or high melting  
6 point metals. A characteristic feature of this process is a brittle, porous and rough recast layer on machined  
7 surfaces, which undermines integrity and limits its applications. Previous attempts to remove the recast have  
8 increased process steps and complexity, and in the case of EDM ECM hybrid processes have failed to understand  
9 or explain process mechanisms and have not proposed methods to control removal mechanisms to produce tailored  
10 surfaces. Here, we introduce tailored electrolytic-dielectrics that eliminate the defective recast layer, while  
11 maintaining machining rate. By adding selected electrolytes to a conventional deionised water dielectric in a  
12 standard EDM machine, material removal mechanisms can be altered and controlled in a simultaneous electrical  
13 discharge and electrochemical process, producing discrete surface morphologies through passive oxidation,  
14 aggressive pitting, and electro-polishing. These bespoke dielectrics alter fundamental machining behaviour to  
15 alternate between conventional EDM discharging and electrochemical dissolution. For the first time, it is shown  
16 that machining rate can be maintained while reducing, and eliminating, the defective EDM recast layer, which  
17 would otherwise need removal, in a single step process that combines the accuracy of EDM with the surface finish  
18 of ECM with the potential to produce high integrity surfaces with high throughput. The mechanisms behind this  
19 unique machining process are described through fundamental waveform and discharge analysis, which revealed  
20 discrete pulse types and their significance to the process, the importance of pulse ratio balance, the time-varying  
21 nature of the process, and the significance of high-voltage regions to electrochemical removal. Key process  
22 parameters are determined, such as EDM: ECM pulse ratio balance, electrolytic-dielectric conductivity, salt type,  
23 machining/exposure time, and electrode/servo advance, which are crucial to producing tailored surfaces. A model  
24 is devised to describe the overall balance between discharge based and dissolution based removal. Through this  
25 model, the point during machining at which complete recast layer removal occurs is predicted and validated  
26 through experimental analysis. This adapted EDM process has significant potential to be used for producing  
27 recast-free features by using an easily modified dielectric.

28

29 **Keywords:** Recast layer; edm; hole drilling; zero recast; hybrid;

## 30 1. Introduction

31

32 Electrical discharge machining (EDM) is a non-conventional machining process used to machine hard, high  
33 melting point conductive materials. EDM is a non-contact process which uses thermal energy to remove material,  
34 enabling machining regardless of the material's mechanical properties. One drawback of EDM is the formation  
35 of a rough recast surface layer containing porosity, cracks, contamination, and oxides, which can affect the  
36 functional properties of the machined part.

37 Although the recast layer and its defects can be minimised through careful and lengthy parameter and process  
38 optimisation at the penalty of reduced machining rate [1], the recast layer cannot be eliminated from EDM surfaces  
39 without post-machining removal. This removal is critical for applications where surface integrity is crucial to part  
40 performance. Such removal methods include grit blasting [2, 3] and magnetic abrasive machining [4, 5]. These  
41 methods increase production cost considerably and the resulting surfaces may have increased roughness and  
42 embedded particles [6], which also impacts part performance.

43 Electrochemical machining (ECM) is an alternative non-conventional machining process which can produce high  
44 integrity surfaces without recast layers. However, in some applications such as high aspect ratio holes, EDM is  
45 preferred due to machining accuracy and higher removal rate. In ECM, anodic dissolution causes removal of  
46 workpiece material, driven by an applied voltage between the workpiece and a cathode tool, in an electrolyte that  
47 is usually an aqueous salt solution (e.g. NaCl, NaNO<sub>3</sub>) [7]. The metals in the workpiece give up electrons  
48 (oxidation) to the electrolyte ions (reduction), which are usually salts, and are lost into the workpiece. They can  
49 also form metal hydroxides when reacting with OH<sup>-</sup> [8, 9]. Post-process electrolytic removal can also be used to  
50 remove EDM recast layers via electrochemical dissolution [10, 11]. Once again however this approach adds  
51 significant time and cost to the overall process chain.

52

53 2-step combination processes of EDM and ECM within the same machine tool have been demonstrated to  
54 eliminate the recast layer. An example of this is a two-step wire EDM (W-EDM) removal method where first a  
55 surface is machined with EDM to allow high bulk material removal rates, after which the gap is changed and  
56 electrolyte is used to remove the recast layer [12]. However, this setup involves a change of electrolyte and  
57 effectively combines two distinct processes in a process chain. The adaptation to machine architecture to distribute  
58 both electrolyte and dielectric should not be underestimated.

59

60 A similar process using disks to cut material was used in a sequential EDM-ECM process in the same machine  
61 tool [13], in which the recast layer was shown to be removed via cracking at micro-cracks due to tensile stress,  
62 bubbles, and fluid flow. Once again, this process involved removal of the EDM oil and replacement with an ECM  
63 electrolyte, and therefore is a complex arrangement difficult to implement in a regular production system. It is  
64 clear that electrochemical methods are particularly effective in recast layer removal given the absence of a  
65 deformed layer from mechanical methods, or a heat-affected layer from thermal methods. It is therefore of interest  
66 to utilise the anodic dissolution electrochemical removal mechanism to produce a metallurgically ideal surface.  
67 EDM dielectrics have the potential to be exploited as a delivery mechanism for electrolyte type fluids to enable  
68 ECM and EDM in a combined process. Processes that combine electrochemical and electrical discharges (ECDM)  
69 have been explored previously, mainly to machine non-conductive materials [14] using NaOH, KOH, or NaNO<sub>3</sub>  
70 at high conductivities (10 mS/cm to 100 mS/cm) [15, 16]. In ECDM, a gas layer is produced over the cathode due  
71 to cathodic hydrogen generation via the electrolysis of water. This gas layer then acts as a dielectric, which when  
72 in the vicinity of a non-conductive material, can cause an electrical discharge between the electrode and the gas  
73 interface which causes melting and vaporisation of the material. At the same time, electrochemical dissolution  
74 can aid material removal. This process has also been used for the machining of conductive material in high  
75 conductivity liquids [17], however as discharges are the main mechanism of material removal, recast layers are  
76 still present on the machined surface.

77

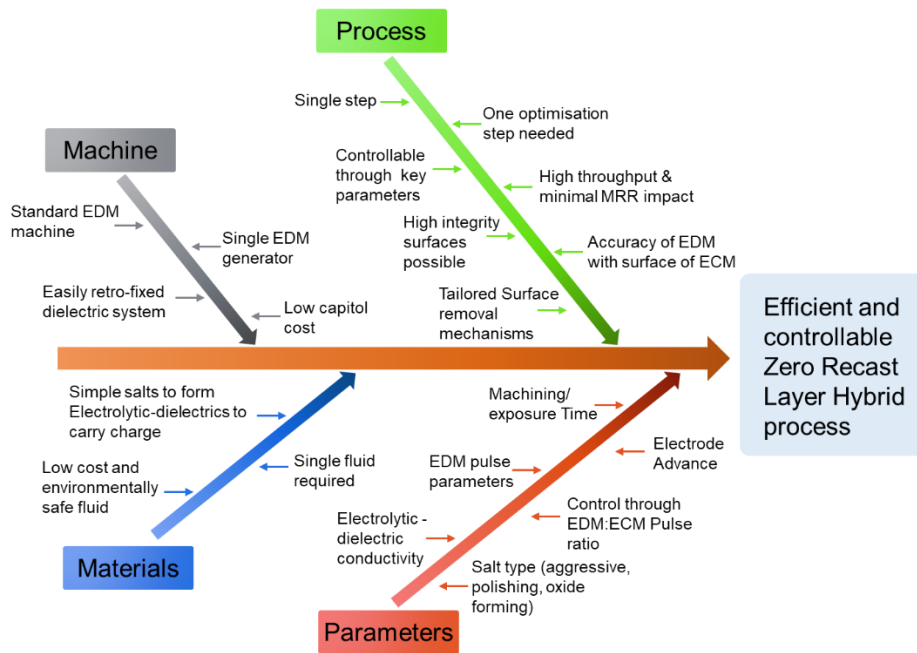
78 In ECDM, other adaptations have been made in an attempt to reduce the size of or remove the recast layers in this  
79 combined process. The recast layer can be somewhat reduced using lower conductivity fluids, as shown by Zhang  
80 et al. [18, 19] at conductivities from 4000  $\mu$ S/cm to 10,400  $\mu$ S/cm), while Zhang et al. [20] also showed some  
81 evidence that some recast layer could be removed after sufficient time. However, the evidence for this is poor and  
82 the work does not attempt to explain the mechanisms nor attempt to balance the contribution of ECM and EDM  
83 in process to propose methods to control resulting surfaces and process characteristics. The use of EDM combined  
84 with ECM has so far only been observed in a superficial manner, with material removal rate (MRR), tool wear  
85 and macro-scale surface features being explored. However, to the best of our knowledge, no attempt has been  
86 made to interrogate the impact of a conductive dielectric on the spark-dissolution balance, removal mechanisms,  
87 surface morphology, or attempt to explain process behaviour.

88

89 By combining EDM and ECM removal mechanisms in a single controllable process by use of electrolytic-

90 dielectrics the machining steps are reduced from at minimum two to a maximum of one step, and on a single  
91 standard EDM machine with only an EDM generator. This reduces capital cost, increases throughput, reduces  
92 optimisation steps, and can easily be retro-fitted to existing machines by replacing DI with electrolytic-dielectrics.  
93 The proposed method also has the advantageous ability to produce high aspect ratio holes quickly with no surface  
94 damage. Interaction between the EDM and ECM side is expected and will affect processing speed and surface  
95 morphology. The capability to produce a controlled and tailored surface with no recast by exerting control over  
96 the spark and anodic dissolution balance is needed. Our work will approach this by demonstrating and advancing  
97 the state-of-the-art by investigating the hybrid process from a fundamental basis, concerning the balance of pulses  
98 between electrical and electrochemical removal. This will also be linked to the discrete electrochemical  
99 dissolution mechanisms caused by different salts and conductivities, which heavily influence surface  
100 characteristics, such as passive oxidation, aggressive pitting, or electro-polishing. Analysis of the recast layer,  
101 removal rate, and surface analysis will be conducted to relate fundamental understanding to quantifiable  
102 machining process output factors used in industry. Waveform analysis is used to understand process mechanisms  
103 and differences between electrolytic-dielectrics, and is used to reveal discrete pulse types. Key process parameters  
104 which are crucial to producing tailored surfaces are determined, such as ~~EDM:ECM pulse ratio balance~~,  
105 electrolytic-dielectric conductivity, salt type, machining/exposure time, ~~and~~ electrode/servo advance. **The**  
106 **EDM:ECM ratio was also determined to be crucial to process behaviour, and although it is currently not directly**  
107 **controllable in a parametric sense, indirect control of this parameter was determined to be significant for future**  
108 **control.** A mathematical and validated model will be used to illustrate the overall process balance through  
109 fundamental electrochemical theory and process pulse data, thereby allowing more generic and transferable data  
110 to be utilised by the machining user base in both academic and industrial settings.

111 Fig. 1 shows a causal diagram representing the main aspects of the process and it's novelty, resulting in the zero  
112 recast hybrid process.



113

114 Figure 1. Causal Diagram showing main causes and components of the proposed process which result in novel  
 115 zero recast layer hybrid process

116 **2. Experimental**

117

118 **2.1. Materials**

119 The workpiece was an Inconel 718 rectangular piece (nominal dimensions 25 mm by 25 mm), which is used in  
 120 high-temperature aerospace applications due to its resistance to corrosion and good high-temperature properties  
 121 [21, 22]. The nominal composition of Inconel 718 is listed in Table 1. The theoretical electrochemical equivalent  
 122 for the alloy, calculated for the upper and lower ranges of the nominal composition as shown in Table 1, was  
 123 calculated as 0.258 – 0.295 mg/C according to  $\frac{m}{Fz}$ , where  $F$  is the Faraday constant,  $m$  is the atomic mass, and  $z$   
 124 is the ion valency.

125

126 Table 1 - **Nominal composition of Inconel 718.** Inconel 718 workpiece used in all experiments. Composition  
 127 also used in ECE calculation.

Element	Ni	Cr	Nb	Cu	Mo	Ti	Al	Co	Ta	Si	Mn	Fe	Total
Min Wt %	50	17	4.75	0	2.8	0.65	0.2	0	0	0	0	24.6	100
Max Wt %	55	21	5.5	0.3	3.3	1.15	0.8	1	0.05	0.35	0.35	11.2	100

128

129 Deionised water (DI) of conductivity 1  $\mu\text{S}/\text{cm} \pm 0.5 \mu\text{S}/\text{cm}$  was produced using the external dielectric filtration  
 130 unit on the machine, consisting of a cartridge filter, resin deionisation unit, and ceramic filter. Electrolytic  
 131 conductivity was measured using a Mettler-Toledo S3 conductivity meter before machining. Electrolytic-

132 dielectrics were produced using the deionised water mixed with the selected salts, using a magnetic stirrer until  
133 the conductivity reading stabilised and the required levels for experimentation were obtained.

134

135 To show the principles of machining and recast layer using electrolytic-dielectrics, five electrolytic conductivities  
136 were used to assess the effect of conductivity and increased electrochemical action on the EDM recast layer.  
137 Conductivities of 1, 200, 400, 600, 800, and 1000  $\mu\text{S}/\text{cm} \pm 1 \mu\text{S}/\text{cm}$  were used, using NaCl (Fisher Scientific,  
138 >98%). These electrolytic conductivities, which are an order of magnitude greater than conventional EDM  
139 dielectrics, and an order of magnitude lower than conventional ECM electrolytes, were selected to allow both  
140 anodic dissolution and discharges thus enabling both modes of materials removal.

141

142 To manipulate the electrochemistry of electrolytic-dielectrics to control surface morphology, six different sodium  
143 salts were chosen to observe differences in electrochemical action of the anions on the EDM recast layer. NaCl  
144 (chloride),  $\text{NaHCO}_3$  (carbonate),  $\text{NaNO}_3$  (nitrate),  $\text{Na}_2\text{SO}_4$  (sulfate),  $\text{NaNO}_2$  (nitrite), and  $\text{Na}_2\text{SO}_3$  (sulfite) were  
145 used at 600 and 1200  $\mu\text{S}/\text{cm}$ . All salts were purchased from Fisher Scientific and were >98% purity.

146

## 147 2.2 Machining method & Equipment

148 Machining experiments were performed on a GF+ DRILL 2009. The electrodes used were 1.9 mm diameter brass,  
149 due to its lower wear and improved MRR compared to Cu, with a multi-hole deionised water channel to ensure  
150 no central material remains after machining.

151 Constant electrode rotation (36 RPM) was used to ensure even wear, machining depth, and hole profile. Internal  
152 electrode flushing was used for all trials using the in-built high-pressure pump at 5 MPa, set manually through the  
153 machine pump pressure gauge. Low pressure surface flushing was used throughout machining to ensure that the  
154 electrode and machining surface were submerged, especially at the start of machining.

155 Prior to machining with each dielectric, the tool electrode was redressed on a graphite surface using DI to remove  
156 electrode curvature. After this, the dielectric was switched to the electrolytic solution and the fluid system flushed  
157 to ensure correct conductivity levels.

158

159 Machining using was conducted for a fixed time of 60 seconds, with three repeats per conductivity level to show  
160 the principles of machining and recast layer using NaCl. 40 seconds of machining time was selected to manipulate  
161 the electrochemistry of electrolytic-dielectrics using various salts, which was selected due to the depth limitation

162 of the Inconel 718 workpiece. Control holes machined using DI were also drilled for comparison.  
163 EDM parameters were fixed during experimentation and were set to 18 A peak current, 5  $\mu$ s on-time, and 10  $\mu$ s  
164 off-time, which were chosen as they produced good MRR and wear performance with the DI dielectric. MRR was  
165 calculated via the electrode servo depth-time graphs generated from the EDM machine and the wear value, which  
166 was measured by electrode z-axis difference using a reference surface, before and after machining. By subtracting  
167 the wear from the machine depth as shown in the machine depth-time graphs, a hole depth value can be calculated  
168 and by using the machining time a rate can be calculated in mm/s.

169  
170 For the process model, current efficiency was calculated by first machining a hole with DI to produce a generalised  
171 EDM surface exhibiting an altered recast layer serving as a baseline for this study. Following this, the dielectric  
172 was altered to a 1200  $\mu$ S/cm sulfite dielectric and the same electrode was lowered into the hole. The same pulse  
173 parameters used were used. Electrode advance speed was minimised so that no electrical pulses were observed on  
174 the oscilloscope, as the electrode was essentially stationary in the hole. This results in the pulses causing  
175 electrochemical machining on the surface of the hole. The amount and charge of pulses were recorded for use in  
176 the model.

177

### 178 2.3. Sample Preparation and characterisation

179 To view the machined surface, holes were sectioned through the centre axis of the holes using an abrasive cutting  
180 disk and then manually ground to reach the centre of each hole. They were then mounted and polished to a mirror  
181 finish and then etched using V2A etchant (100 ml water, 100 ml hydrochloric acid, 10 ml nitric acid) to reveal the  
182 recast layer.

183 For calculating the current efficiency with increased accuracy, the holes were drilled in the centre of a two-part  
184 parallel workpiece clamped together to accurately assess the total material removed.

185

186 An Alicona G4 focus variation instrument was used to image and quantify the surface roughness of the machined  
187 surface (20X objective). The surface datasets were separated into roughness and waviness profiles using a  
188 Gaussian filter with cut-off 250  $\mu$ m to effectively remove the hole curvature from the scanned surfaces for  
189 improved roughness comparison using the Sa roughness parameter. The overcut of the holes were also measured  
190 using the Alicona G4, and was stated as a percentage increase compared to the 1.9 mm electrode used to machine  
191 the holes. **The overcut is defined as the increase in entrance hole diameter, which is always the largest increase in**

192 diameter across the hole, as compared to the size of the 1.9 mm electrode. The overcut is calculated as the resulting  
193 entrance hole diameter minus the size of the electrode, and converted to a percentage increase. The change in  
194 roughness with depth was obtained by separating the lateral profiles along the depth of each hole and calculating  
195 Ra. The resulting change in Ra with depth curve was smoothed by a moving mean method with a smoothing factor  
196 of 1.5, processed in Matlab, to ease figure understanding. This was then plotted with different conductivities using  
197 NaCl.

198 Blind holes were machined instead of through holes to increase process understanding through EDM and ECM  
199 zone data, as through holes may result in significantly reduced or no EDM zone depending on process method.

200 Backscattered (BSE) and secondary electron (SE) microscopy using the FEI Quanta600 SEM were taken of the  
201 hole surfaces to assess the influence of the salt and conductivity on the recast surface. Recast layer depth  
202 measurements were obtained by calculating the recast layer area for 15 SEM areas of 90 by 80  $\mu\text{m}$  and dividing  
203 the length of each area to obtain an average recast layer measurement.

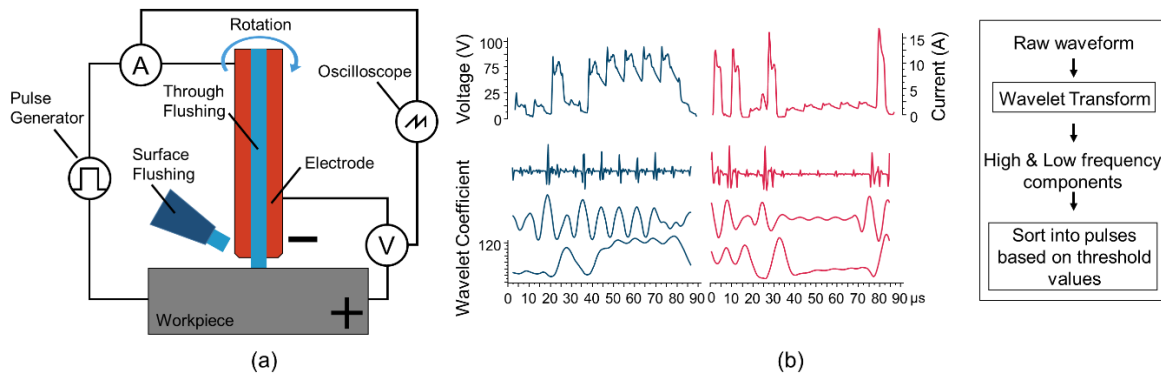
204 For the process model, 3D profilometry using the Alicona G4 was used to measure total volumes removed by  
205 EDM and electrochemically mechanisms on both sides of the holes. This total volume was converted to mass  
206 using the density of the material. The material removed was compared to that calculated by Faraday's Law using  
207 the total charge measured to calculate the true current efficiency, which was then used in the model.

208

#### 209 2.4. Waveform measurement and processing

210

211 Waveform analysis was conducted to measure the proportion of different types of pulses in machining as shown  
212 in Fig. 2a. A Pearson current monitor model 150, with 0.5 V/A sensitivity was used to measure the current  
213 waveforms. A Rohde & Schwarz RT-ZD01 high-voltage differential probe with 100 MHz bandwidth at 1000:1  
214 attenuation rating was used to measure the voltage waveforms. A Rhode and Schwarz RTB2000 oscilloscope with  
215 sample rate of 2.5 G sample/s and bandwidth of 70 MHz was used to process the current and voltage data.  
216 Waveform data was measured for 1.2 seconds at three instances for each dielectric, at 3, 20, and 35 seconds after  
217 the start of machining. Due to the size of the data set (2,000,000 points) and inability to record data continuously,  
218 1.2 seconds were recorded at 166,670 Samples/s of machining at three instances to assess the change in pulse type  
219 ratios with machining time and depth.



220

221 **Figure 2 – Waveform and pulse analysis.** a) Experimental setup for capturing waveforms using an  
 222 oscilloscope, current sensor, and voltage probe. b) Method of discriminating waveform pulses based on  
 223 amplitudes of wavelet transform

224 Waveform data was analysed in Matlab. Pulse start and end points were calculated by differentiating the  
 225 waveform, revealing large changes in voltage and current which relate to pulse start and end times. Pulse  
 226 discrimination was achieved using the discrete wavelet transform with the Daubechies wavelets, which matches  
 227 well with EDM waveforms in terms of shape [23]. The wavelet transform utilises a wavelet, which is a finite  
 228 length oscillating wave which starts and ends with zero amplitude, to separate a signal by its frequencies. By  
 229 compressing a wavelet in the time domain using the scaling factor in the wavelet transform and shifting it across  
 230 the length of a signal, it is possible to extract the high frequency components [24]. Similarly, by stretching the  
 231 wavelet and shifting it across a signal it is possible to extract the low frequency components, shown in Fig. 2b.  
 232 By using the amplitude values from the transformed voltage and current waveforms and comparing them against  
 233 threshold values, it is possible to count and discriminate pulses into different types. Threshold values must be  
 234 manually chosen by first understanding which types of pulses are present in the raw current and voltage data, and  
 235 then relating the different types of pulses to the values of the corresponding wavelet transformed pulses by manual  
 236 sampling. The exact values of the ranges will differ when electrical parameters and experimental equipment are  
 237 changed. In this way, if the threshold condition for both the current and voltage is met for a certain pulse type the  
 238 pulse can be automatically categorised. Different pulse types have discrete thresholds, for example an  
 239 electrochemical pulse will have a very high voltage and a very low current, while an EDM pulse will have a  
 240 medium voltage and medium current, and a semi-arc pulse will have a low voltage and high current. By going  
 241 through each pulse sequentially and comparing to these discrete pulse signatures, pulses can be categorised. The  
 242 wavelet transform allows this signature to be more easily categorised by essentially simplifying the waveforms to  
 243 reveal clear pulse signatures. The ratio of pulses was then calculated at 3, 20, and 35 seconds, as well as the overall  
 244 ratio for all three periods.

245 High voltage regions were measured by counting areas of sustained high voltage (ignoring smaller regions of high  
246 voltage due to discharge delay) and comparing to normal machining waveforms.

247

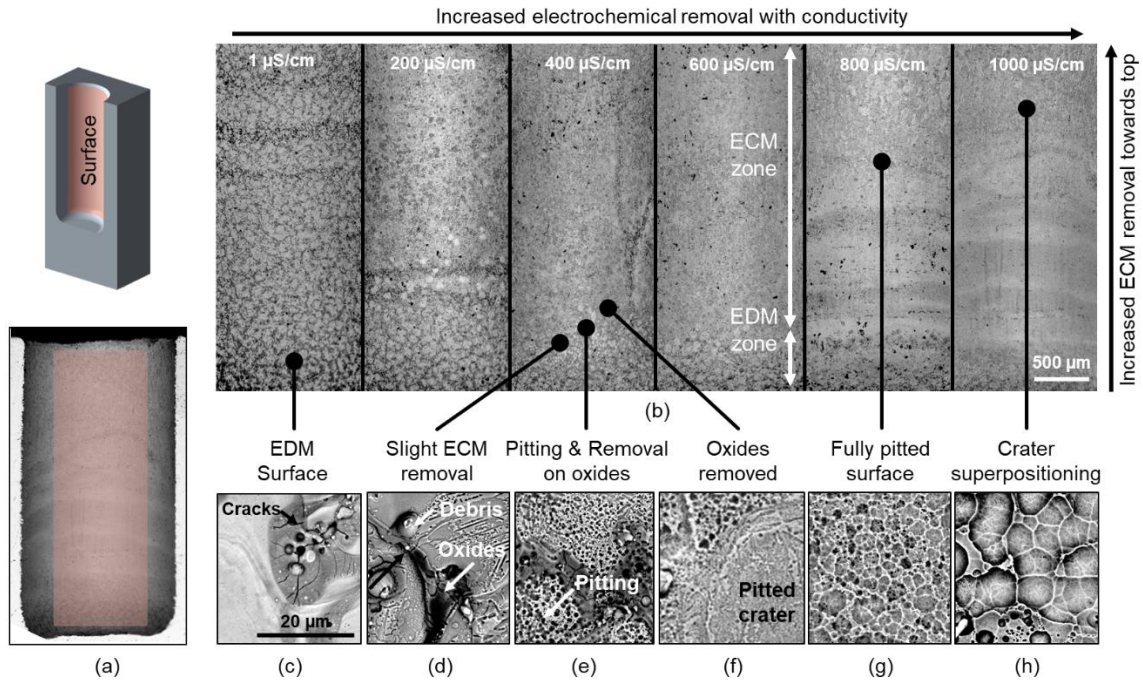
### 248 3. Results

249

#### 250 3.1. The principles of machining and recast layer removal using electrolytic-dielectrics

251

252 Fig. 3 shows holes machined using NaCl formed electrolytic-dielectrics at varying conductivities, at the EDM  
253 parameters of 18 A peak current, 5  $\mu$ s on-time, and 10  $\mu$ s off-time. The surface view of the holes is shown in Fig.  
254 3a. Fig. 3b shows the surface of the machined holes, with higher magnifications shown in Fig. 3c-h. The surface  
255 of the DI machined hole is covered with typical recast layer features such as re-solidified material, workpiece and  
256 electrode debris, cracks, and oxides, as shown in Fig. 3c. The oxides are shown by the darker regions which  
257 usually surround the craters, while the lighter regions correspond to re-solidified material (craters). When the  
258 conductivity is increased to 200  $\mu$ S/cm by increasing chloride anions available for electrochemical action, at the  
259 same EDM parameters, the surface shows two distinct zones. The upper region exhibits a zone in which the surface  
260 morphology is evidently dominated by electrochemical removal, whilst the lower zone still exhibits a  
261 characteristic EDM surface. The division between the EDM dominated zone and the electrochemical dominated  
262 zone is not step-wise, instead a transition occurs in which EDM pits decrease in frequency from the bottom of the  
263 hole towards the top. The bottom of the transition zone has a surface fully covered with EDM craters with minimal  
264 signs of electrochemical removal, while the top of the transition zone has a surface with no recast layer due to  
265 electrochemical removal. The centre of this transition zone is therefore defined as the separation between the  
266 EDM and ECM zone and is used to calculate the EDM zone ratio, determined manually through SEM images  
267 which clearly show the transition zone, as shown in Fig. 4. Although recast layer cross sections may aid in  
268 determination of the zero-recast point, due to the variable nature of the surface a single cross-section is not precise  
269 and may not be accurate, and as it is not possible to take several cross sections of the same hole due to the small  
270 size, surface SEM and roughness data which produce data over the entire surface are a necessary compromise. In  
271 this case, electrochemical removal has resulted in pitting of the recast layer through anodic dissolution resulting  
272 in its removal. The hole-depth of the discharge-dominated zone decreases with increased conductivity from 36%  
273 at 200  $\mu$ S/cm to 11% at 1000  $\mu$ S/cm as shown in Fig. 4, due to the increased dissolution with increased  
274 conductivity.

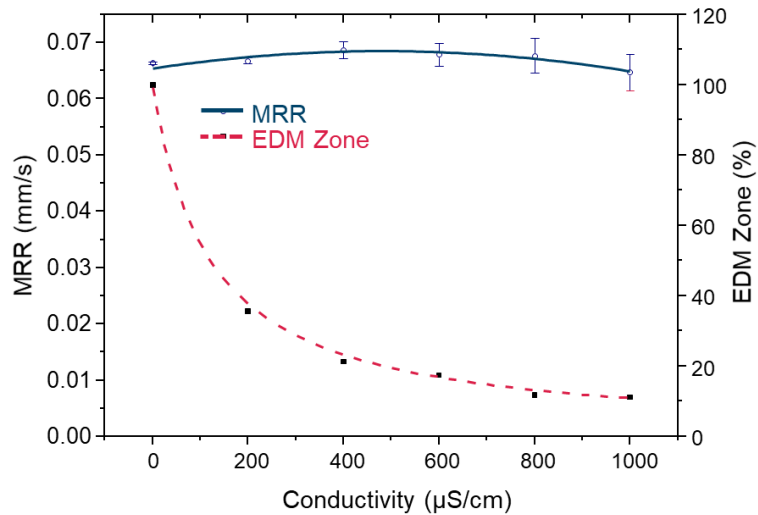


276

277 Figure 3 – **Dissolution behaviour through SEM analysis.** SEM back-scattered images showing the recast  
 278 surface of EDM holes. (a) Figure showing SEM view used in oxides Fig. 3b-h and image of an entire hole and  
 279 corresponding surface used. (b) Holes from 1 to 1000  $\mu\text{S}/\text{cm}$  conductivity using chloride to induce  
 280 electrochemical dissolution. (c-h) High magnification micrographs of the surface showing increased chemical  
 281 action. 3 holes were machined at each conductivity level.

282 Gradual electrochemical removal from the discharge zone to the dissolution zone is shown through Fig. 3c–h,  
 283 which takes place along the hole axis, and with the increase in conductivity from 1 to 1000  $\mu\text{S}/\text{cm}$ . Slight  
 284 electrochemical removal can be observed in Fig. 3d. At this level however the EDM surface oxides are not  
 285 removed. Increased electrochemical removal causes pitting and cracking of the oxides (Fig. 3e), followed by  
 286 removal of all oxides (Fig. 3f), and finally a homogeneous surface with the entire recast layer removed (Fig. 3g,h).  
 287 The pit diameter is shown to increase from less than 1  $\mu\text{m}$  to 5  $\mu\text{m}$  at 1000  $\mu\text{S}/\text{cm}$ .

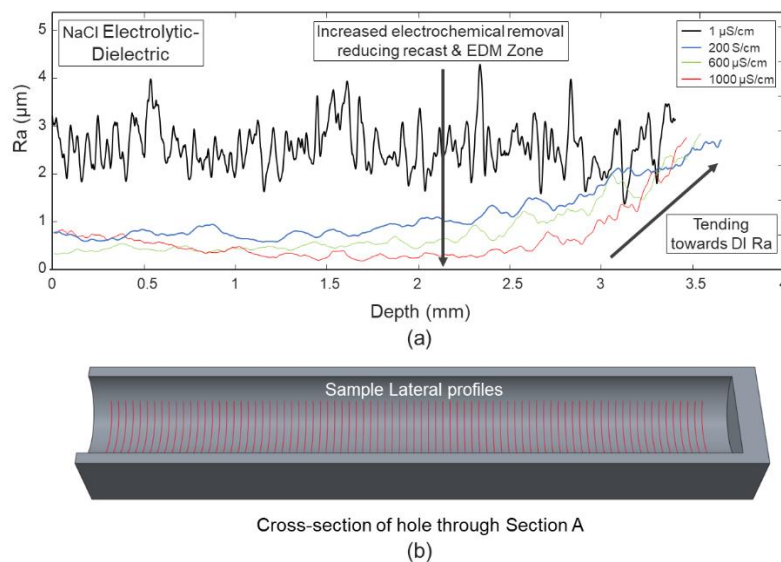
288



289

290 Figure 4. **MRR and EDM zone data.** Change in MRR and the EDM Zone (area dominated by EDM discharges  
 291 compared to the ECM removed area) with conductivity, using NaCl to enable dissolution at five conductivity  
 292 levels. MRR error bars represent  $\pm$  SD from mean  $n = 3$ .

293 The increase in conductivity was also shown to have little influence on the overall material removal rate (MRR),  
 294 shown in Fig. 4, which implies that ECM removal has a very limited influence on the EDM removal mechanisms,  
 295 however with increasing conductivity a decreasing trend can be seen after 600  $\mu$ S/cm. The EDM Zone was also  
 296 shown to decrease with an increase in conductivity due to increased electrochemical strength.

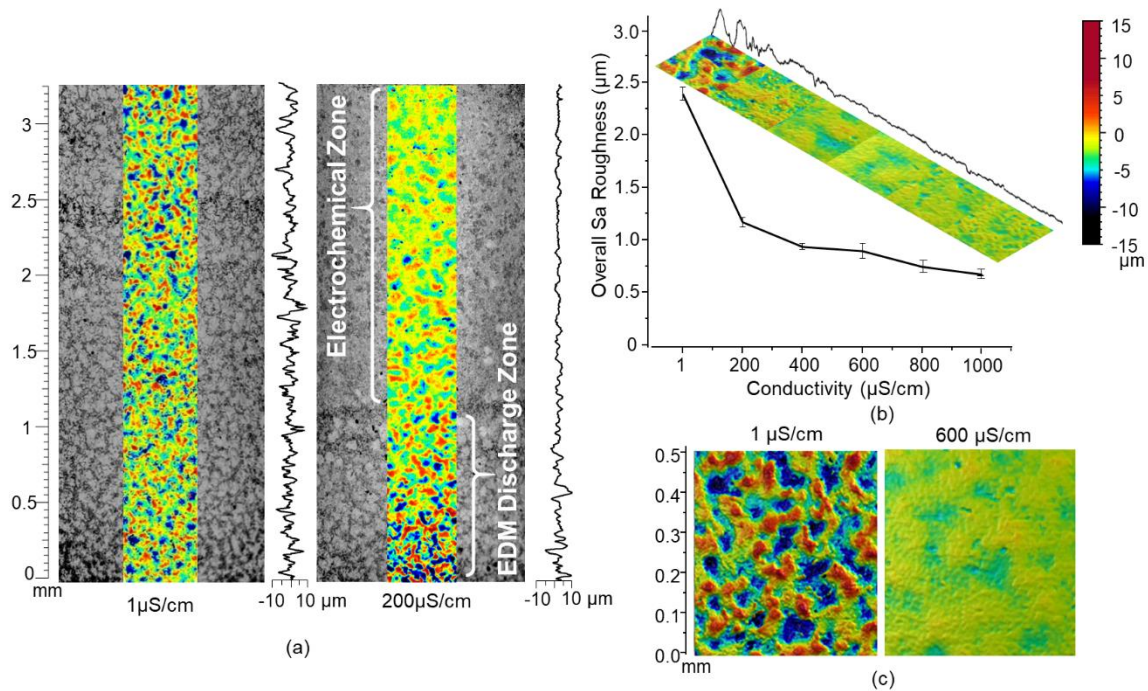


297

298 Figure 5. **Clarifying the EDM and ECM zone through roughness analysis.** (a) Effect of NaCl conductivity on  
 299 the change in roughness with depth, showing two distinct roughness zones corresponding to the EDM and ECM  
 300 zones (b) Diagram clarifying locations of sampled lateral profiles.

301 Fig. 5 shows a comparison of the change in Ra roughness along the depth of holes machined with NaCl  
 302 electrolytic-dielectrics at 1, 200, 600, and 1000  $\mu$ S/cm (400 and 800  $\mu$ S/cm omitted for figure clarity). An increase  
 303 from 1 to 200  $\mu$ S/cm causes a profile with a considerably reduced roughness, with two distinct zones. The top

304 portion has a low roughness, which at 1.5 – 2 mm depth begins to rapidly increase tending towards the roughness  
 305 of DI. By comparing to Fig. 3 and Fig. 4 we can correspond this to the EDM and ECM zones, relating the presence  
 306 of EDM craters to the increased roughness and the smoothing of electrochemical removal to the decreased  
 307 roughness. An increase in conductivity increases electrochemical strength causing more recast removal and  
 308 smoothing and increasing the length of the low roughness ECM zone. NaCl at 1000  $\mu\text{S}/\text{cm}$  shows a significantly  
 309 reduced roughness and only begins to increase in roughness between 2.5 – 3 mm. The change in roughness data  
 310 thus shows increased ECM removal in the ECM zone due to surface smoothing and increased roughness in the  
 311 EDM zone due to electrical discharges. Although this data shows recast removal through surface smoothing, it  
 312 cannot be used to obtain the EDM zone or the zero recast point as it only shows a change in roughness. Thus SEM  
 313 images, which clearly show craters and electrochemically removed surface, are currently the preferred method.  
 314 The change in roughness along the holes is shown in Fig. 6a for the 200  $\mu\text{S}/\text{cm}$  hole as compared to DI, which  
 315 shows that the roughness increases along the hole until the EDM discharge zone where the roughness tends  
 316 towards a hole machined with DI. Fig. 6b shows the decrease in roughness with an increase in dielectric  
 317 conductivity. Fig. 6c shows a clear comparison in surface roughness between an EDM surface and an  
 318 electrochemically smoothed surface. Although the volume of material removed from the recast layer was not  
 319 analysed, it can be assumed that a decrease in roughness, i.e. anodic levelling, correlates to increased material  
 320 removed from the recast layer.



321

322 Figure 6. **Roughness analysis of surfaces.** (a) Roughness for 1 and 200  $\mu\text{S}/\text{cm}$  hole surfaces showing the SEM

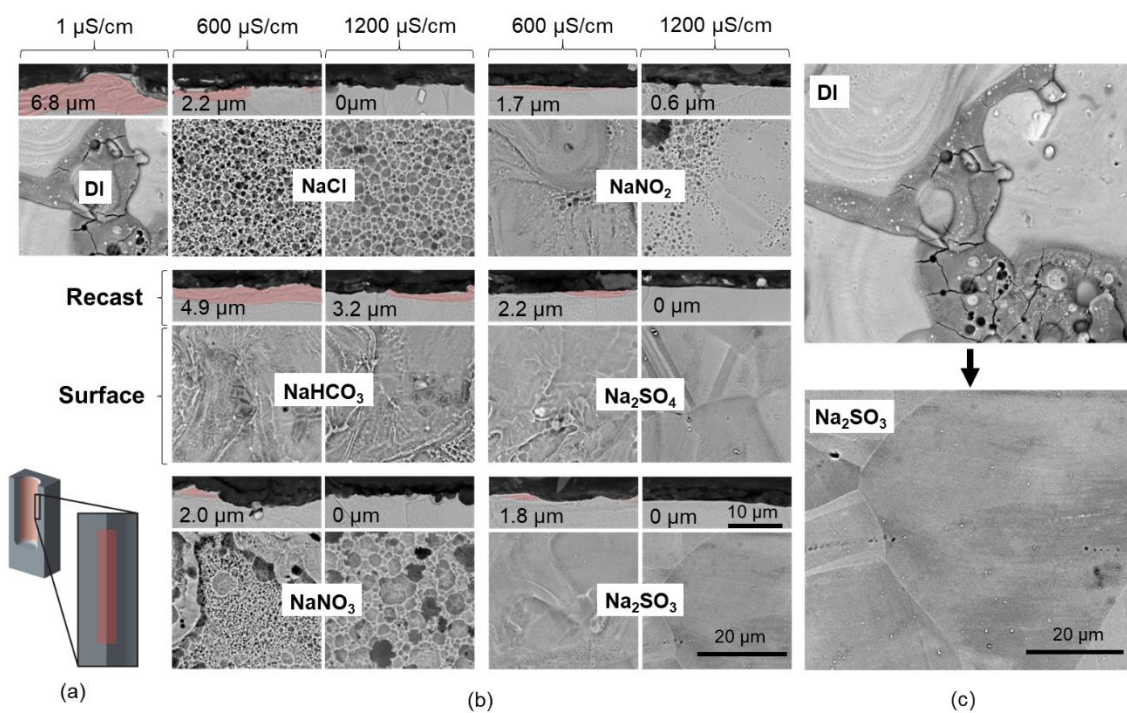
323 surface overlaid with a 3D surface height map and accompanied by a profile section height map. b) Showing the  
 324 change in roughness with conductivity in Sa with accompanying 3D/2D surface maps to visually show the  
 325 change. Roughness error bars represent  $\pm$  SD from mean  $n = 3$ . C) A close up of the difference between two  
 326 conductivity levels caused by dissolution.

327 3.2 **Manipulating the electrolytic-dielectric conductivity and composition to control surface morphology**

328

329 Using NaCl, it was shown that electrochemical removal during EDM hole drilling can result in a hole with zero  
 330 recast layer along the majority of the hole, at the EDM parameters of 18 A peak current, 5  $\mu$ s on-time, and 10  $\mu$ s  
 331 off-time. In the case of chloride anions, anodic dissolution occurs by aggressive electrochemical pitting, which  
 332 rapidly removes material. Within conventional ECM, both the current density distribution and the electrolyte can  
 333 be altered to allow a higher degree of control over the material removal mechanism and ensure a high surface  
 334 quality is generated [25, 26].

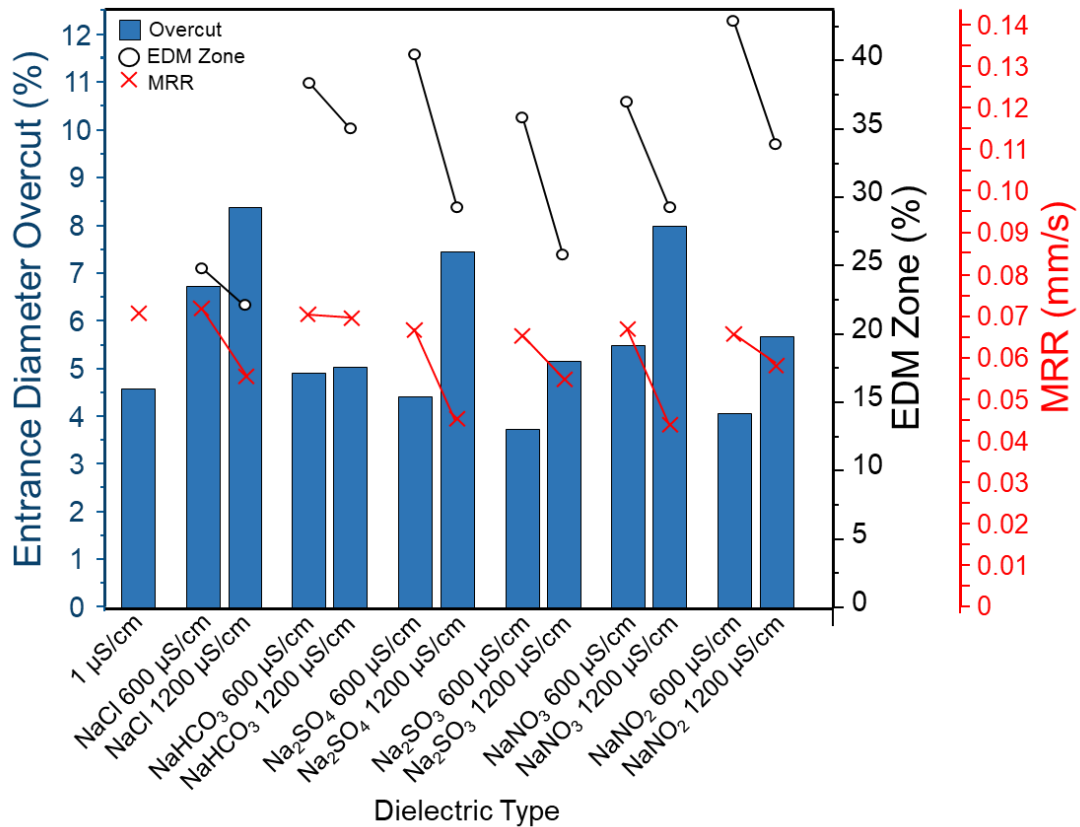
335 Given the limited ability to control the electrical conditions across the inter-electrode gap (IEG) within this hybrid  
 336 setup, different salts were used to control machined surface quality by altering the precise mechanism of  
 337 electrochemical dissolution. With NaCl, aggressive chloride ions result in strong active dissolution. Carbonate  
 338 ( $\text{HCO}_3$ ), nitrate ( $\text{NO}_3$ ), and sulfate ( $\text{SO}_4$ ) were chosen as less aggressive salts capable of forming passivating oxide  
 339 layers when voltages are applied [9]. Nitrite ( $\text{NO}_2$ ) was selected as it is commonly used as an anodic corrosion  
 340 inhibitor due to its ability to form an effective compact passivating layer [27], while sulfite ( $\text{SO}_3$ ) was selected  
 341 due to its application as a corrosion inhibitor by acting as an oxygen scavenger [28].



342

343 Figure 7. **SEM analysis of surface and recast layers.** a) Surface and recast layer views for both 600 and 1200  
344  $\mu\text{S}/\text{cm}$  holes, with recast area highlights in red. b) SEM-BS views of the surface and recast layer of the holes  
345 machined with the salt additives showing average recast layer depth c) Enlarged images of DI compared to  
346 sulfite.  
347

348 Fig. 7b shows that DI of 1  $\mu\text{S}/\text{cm}$  conductivity produces an average recast layer depth of 6.8  $\mu\text{m}$ . At 600  $\mu\text{S}/\text{cm}$ ,  
349 NaCl causes pitting on the recast surface. This pitting removes material from the recast layer to an average recast  
350 layer depth of 2.2  $\mu\text{m}$ , a reduction of 68% from deionised water, while the depth of the hole is the same as  
351 deionised water with a similar MRR as shown in Fig. 8. When the conductivity is increased to 1200  $\mu\text{S}/\text{cm}$  by  
352 increasing the amount of dissolved NaCl, the pitting action increases due to increased concentration of chloride  
353 ions able to transfer charge for material removal. The pit diameter and depth increases, shown in the SEM recast  
354 images in Fig. 7 b, and the entire recast layer is removed. The MRR of the hole, as shown in Fig. 8, is similar at  
355 600  $\mu\text{S}/\text{cm}$  to DI (0.073 mm/s to 0.074 mm/s), however at 1200  $\mu\text{S}/\text{cm}$  the change is more significant, from 0.074  
356 mm/s to 0.057 mm/s (21.6%). This is likely due to the reduction in electrical discharges due to the higher electrical  
357 conductivity and increased charge transferred by anodic dissolution in the electrolytic-dielectric. In both cases,  
358 dissolution of the recast layer shows increased removal along the hole due to increased exposure time.  
359 The EDM zone is seen to decrease with an increase in conductivity, with NaCl having the smallest zone followed  
360 by  $\text{Na}_2\text{SO}_3$ .  $\text{NaHCO}_3$  is shown to have little decrease in EDM zone, while the other electrolytic-dielectrics have a  
361 similar decrease with conductivity. A decrease in MRR also results in a decreased EDM zone for all holes.  
362



363  
364  
365  
366  
367  
368

**Figure 8 – MRR data, EDM Zone percentage, and Overcut.** MRR and EDM zone for electrolytic-dielectrics at 600 and 1200 µS/cm compared to DI, showing a decreasing trend in MRR and EDM Zone at higher conductivities. A corresponding change in entrance hole diameter overcut is stated.

369 NaHCO<sub>3</sub> exhibits a surface with a protective oxide layer. These oxides are spread across the surface as compared  
370 to the EDM oxides, which are concentrated around craters. They can also be inferred to be mechanically weaker  
371 as surface oxides are reduced following sample preparation to view the surface, and no oxides remained after  
372 post-process polishing to view the recast layer, while EDM oxides remained attached. The reduced surface oxides  
373 are shown in Fig. 7b, while an example of an undisturbed NaHCO<sub>3</sub> surface is shown in Fig. 13 (which was cut via  
374 W-EDM to reduce cutting force). This oxide layer is brittle and is prone to cracking, as shown in Fig. 7b by the  
375 darker angular sections and cracked regions, which results in the oxide layer spalling and being removed away by  
376 the high pressure flushing and thermal gradients. Regions of pitting are also observed. The recast layer depth at  
377 600 µS/cm is 4.9 µm with only a 1.5% reduction in MRR compared to deionised water due to the restricted  
378 electrochemical machining of the recast layer, likely due to passive layer formation. An increase to 1200 µS/cm  
379 reduces the recast layer depth to 3.2 µm due to the increased ability to carry charge, with a reduction in MRR of  
380 only 2.6%. In both cases, the MRR is similar to that of deionised water which may be explained by the limited  
381 electrochemical removal due to the oxide layer, in which electrical charge is used in oxide layer formation rather  
382 than material removal.

383  $\text{NaNO}_3$  at 600  $\mu\text{S}/\text{cm}$  produces a complex surface with sections of completely removed recast layer while some  
384 areas are only partially dissolved as shown by the two distinct regions in Fig. 7b, likely due to the variable electrical  
385 conditions within the IEG. The average recast layer depth is 2.0  $\mu\text{m}$  with a reduced MRR of 6.1%. This value is  
386 similar to the recast depth for NaCl, which may be accurate for the chemically removed areas, however due to the  
387 method of measuring average recast depth, by sectioning the hole, it is possible that the true average recast  
388 thickness is larger if all non-removed sections of the recast layer are factored in. When the conductivity is  
389 increased to 1200  $\mu\text{S}/\text{cm}$  the surface is covered by pits and the entire recast layer is removed due to increased  
390 chemical effects.

391  $\text{NaNO}_2$  produces a surface with minimal pitting with no apparent oxides on the surface remaining, however with  
392 some regions with increased pitting due to preferential chemical machining as discussed earlier. Due to this the  
393 recast layer has decreased to 1.7  $\mu\text{m}$  with a reduction in MRR of 7.8%. With an increase to 1200  $\mu\text{S}/\text{cm}$  the recast  
394 layer depth is only 0.6  $\mu\text{m}$  with a reduction in MRR of 18.4% and a similar decrease in MRR compared to  $\text{NaNO}_3$ .  
395 All craters and protrusions have been mostly removed through electropolishing and a surface is produced with  
396 regions of pitted and smooth metal. However, at certain preferential electrochemical machining regions pitting  
397 occurs excessively.

398 The surface of the  $\text{Na}_2\text{SO}_4$  hole is similar to  $\text{NaNO}_2$ , however less recast layer is removed but with minimal pitting  
399 of the surface. Anodic dissolution is thus more uniform and does not form oxides or excessive pitting. At 600  
400  $\mu\text{S}/\text{cm}$  the recast layer depth is 2.2  $\mu\text{m}$  with a reduced MRR of 6.7% compared to deionised water, and a higher  
401 MRR compared to  $\text{NaNO}_3$  and  $\text{NaNO}_2$ . When the conductivity is increased, the recast layer is significantly  
402 levelled with no sign of pitting or oxide layers. Preferential removal at grain boundaries can be seen. The MRR is  
403 also decreased by 35.8%.

404  $\text{Na}_2\text{SO}_3$  has an average recast layer depth of 1.8  $\mu\text{m}$  and no pitting, with a reduced MRR of 8.4%. At 1200  $\mu\text{S}/\text{cm}$   
405 the entire recast layer is removed and a finely polished surface can be seen showing the grain boundaries with no  
406 edge removal in a similar mechanism to  $\text{Na}_2\text{SO}_4$ . In this case the MRR has only reduced by 22.6%.

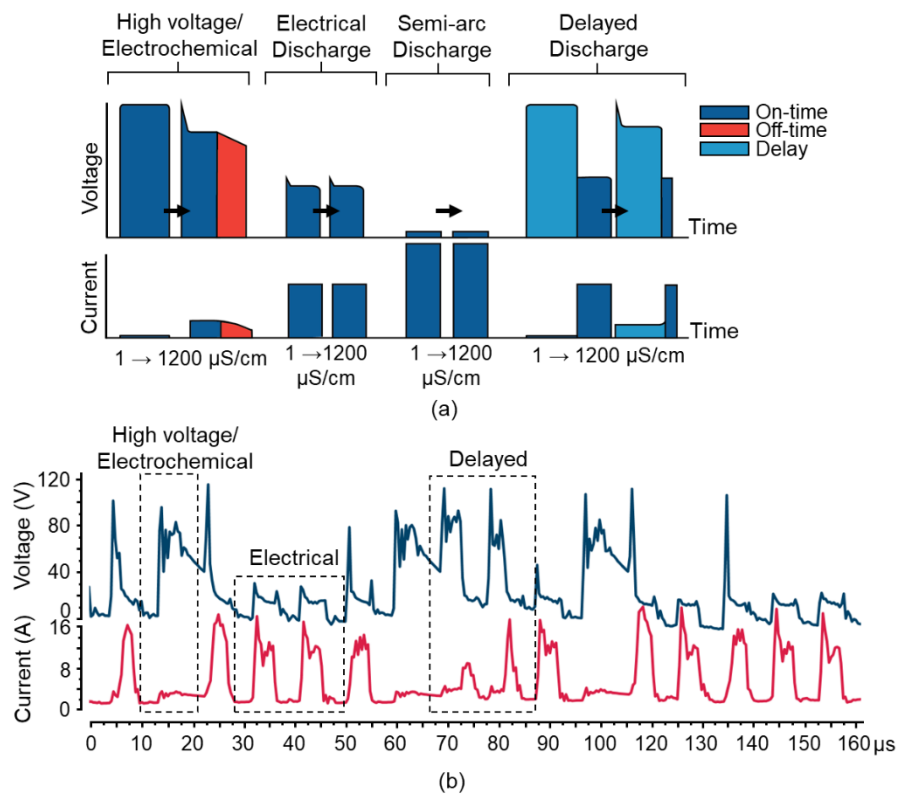
407 The accuracy of the process is shown in Fig. 8, which shows a comparison of the overcuts between the electrolytic-  
408 dielectrics. With an increase in conductivity, the overcut increases, from a minimum of 4 % using  $\text{Na}_2\text{SO}_3$  at 600  
409  $\mu\text{S}/\text{cm}$  to a maximum of 8.4 % using NaCl at 1200  $\mu\text{S}/\text{cm}$ . For comparison, DI produces an overcut of 4.6 %. A  
410 hole with a small EDM zone, which has increased ECM removal, is thus shown to result in a larger overcut.

411

412 3.3. Understanding the influence on process behaviour through waveform and pulse analysis

413  
414  
415  
416  
417

To help understand the different chemical interactions and surfaces produced with different salts, DI, NaCl, NaHCO<sub>3</sub>, and Na<sub>2</sub>SO<sub>3</sub> were used to machine holes, at 600 and 1200 μS/cm. For each hole, waveforms were captured using the set-up shown in Fig. 2a at 3, 20, and 35 seconds after machining.



418

419 **Figure 9. Pulse types found through waveform analysis.** a) Showing the different types of current and voltage  
420 pulses recorded for DI at 1 μS/cm and Na<sub>2</sub>SO<sub>3</sub> at 1200S/cm. b) Showing a captured waveform highlighting  
421 different pulse types.

422 Fig. 9 illustrates the different distinct pulses recorded on the scale of individual discharges. Fig. 9 shows a single  
423 snapshot purposefully selected from the collected waveforms with the different pulse types close together, for  
424 illustration purposes. The high voltage pulse, i.e. where current does not increase to the nominal discharge current,  
425 occurs when voltage breakdown cannot occur due to the breakdown strength of the gap not being overcome,  
426 owing to gap conditions at the instant of the pulse. In deionised water, this results in a high voltage (near-zero  
427 current) pulse. When the conductivity is increased, this high voltage pulse instead causes electrochemical  
428 machining to occur, due to the introduced ions. When a voltage pulse occurs, the voltage first decreases due to  
429 the anodic dissolution current flowing. Once the pulse stops the voltage and current slowly decrease, however  
430 current still flows in the off-time due to capacitance resulting in anodic dissolution in the off-time during this

431 pulse type. The electrical discharge pulse is identical for both deionised water and high conductivity fluids. In this  
432 discharge, high voltage occurs and causes voltage breakdown resulting in current flow. This type of pulse is the  
433 same for both conductivities due to the fact that the discharge gap is full of gaseous products and debris [29], and  
434 thus locally the region can be considered dielectric leading to the breakdown limit being similar to deionised  
435 water. Thus, the frontal area fluid can be interpreted as acting as a dielectric locally, while the fluid on the side  
436 areas acts as an electrolyte. A semi-arc pulse can occur in situations such as when insufficient debris flushing  
437 occurs, fluid dielectric properties are not restored after a pulse, or the discharge gap is too small. This results in  
438 high currents flowing. This is also the same for both deionised water and high conductivity liquids due to only  
439 occurring in the frontal area. Finally, a delayed discharge can occur if a pulse struggles to cause a spark resulting  
440 in a discharge delay, which then finally sparks after a certain time. In deionised water even if the discharge delay  
441 is long, once breakdown occurs the entire pulse duration of a spark still occurs. However, in higher conductivity  
442 liquids the initial discharge delay causes electrochemical machining to occur dropping the voltage and increasing  
443 the current slightly. The machine however recognises this as a pulse and so when discharge occurs the voltage  
444 pulse is stopped prematurely before the entire on-time duration resulting in a combination pulse type. If the  
445 discharge delay is larger than the on-time then no spark occurs.

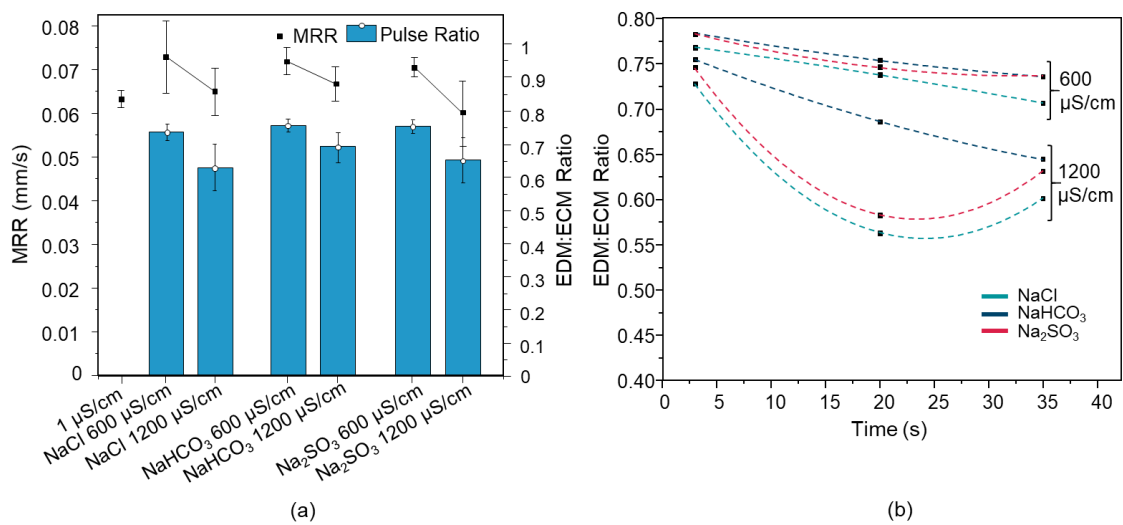
446 Pulses were sorted into pulse types by comparing the values of the wavelet transformed pulses from the current  
447 and voltage waveforms. These values then fit into discrete threshold ranges, which were obtained from sampling  
448 waveform data for different pulse types, and thus were used to classify the pulses. For example, the threshold  
449 range for electrochemical pulse types is between 0.1 and 10 for the current wavelet transformed pulse (the value  
450 is dimensionless as they are wavelet transformed) and between 24 and 100 for the voltage wavelet transformed  
451 pulse. For EDM discharges, the threshold ranges are 15 to 45 and 5 to 40, for the current and voltage wavelet  
452 transformed pulses, respectively. As each type of pulse has a very distinct signature due to the nature of the pulse  
453 voltage and current characteristics, the threshold ranges are discrete and can thus be sorted into certain pulse types.

454 In the EDM ratio calculation, both normal electrical discharges and semi-arc discharges were counted towards the  
455 EDM pulse count, whilst the high voltage type pulses were counted as the electrochemical pulse. To control the  
456 level of electrochemical machining, the amount of high voltage pulses must be controlled as this pulse type is the  
457 main contributor to anodic dissolution.

458 Fig. 10a shows that at 600  $\mu\text{S}/\text{cm}$ , the EDM pulse ratio (EDM pulse count compared to the ECM pulse count), is  
459 76%, 76%, and 74%, and at 1200  $\mu\text{S}/\text{cm}$  65%, 70%, and 63%, for  $\text{Na}_2\text{SO}_3$ ,  $\text{NaHCO}_3$ , and  $\text{NaCl}$  respectively. At  
460 600  $\mu\text{S}/\text{cm}$ ,  $\text{NaCl}$  has the most ECM pulses. Although the difference at 600  $\mu\text{S}/\text{cm}$  is not large due to the low

461 conductivity, at 1200  $\mu\text{S}/\text{cm}$ , the difference is larger and NaCl has the most ECM pulses whilst NaHCO<sub>3</sub> has the  
 462 most EDM discharges. The increase in conductivity thus increases ECM pulse count. As expected, the decrease  
 463 in EDM discharges is also accompanied by a decrease in MRR.

464 Fig. 10b shows that after 3 seconds EDM discharges dominate machining. At 20 seconds at 1200  $\mu\text{S}/\text{cm}$  ECM  
 465 pulses increase due to the increased ECM area, whilst for NaHCO<sub>3</sub> the decrease is less. At 35 seconds for both  
 466 NaCl and Na<sub>2</sub>SO<sub>3</sub> EDM pulses increase. Compared to 1200  $\mu\text{S}/\text{cm}$ , at 600  $\mu\text{S}/\text{cm}$  there are considerably more  
 467 EDM discharges, and the increase in electrochemical pulses is less steep indicating limited anodic dissolution due  
 468 to reduced ions for anodic dissolution.

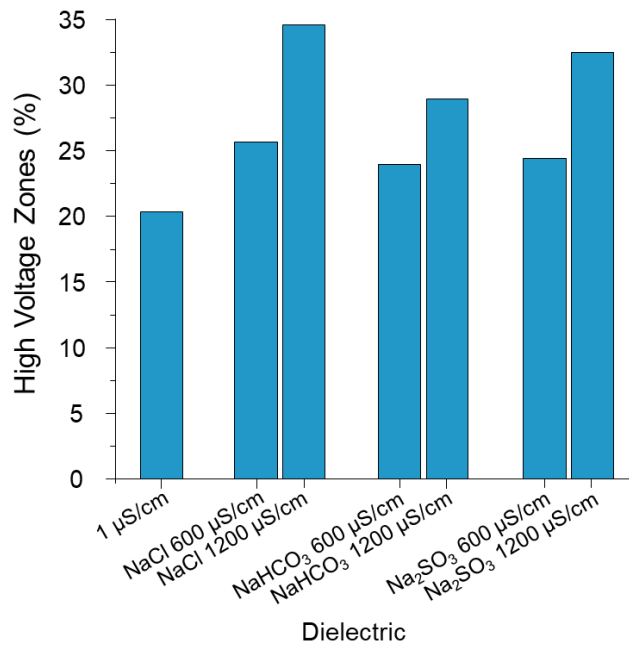


469  
 470 Figure 10. **Pulse balance.** a) MRR and average EDM ratio from all recorded for each additive. MRR and pulse  
 471 ratio error bars represent  $\pm$  SD from mean  $n = 3$ . b) Change in EDM to ECM pulse ratios recorded at 3, 20, and  
 472 35 seconds from start of machining for NaCl, NaHCO<sub>3</sub>, Na<sub>2</sub>SO<sub>3</sub> at 600 and 1200  $\mu\text{S}/\text{cm}$  conductivity.

473  
 474 To further explore the differences in pulses between dielectric solutions, the charges were analysed for  
 475 electrochemical pulses. The average electrochemical pulse charge was similar between the sulfite, chloride, and  
 476 bicarbonate anion solutions, of 7.62, 7.67, and 7.53  $\times 10^{-5}$  C, at 1200  $\mu\text{S}/\text{cm}$  respectively, and 7.46, 7.52, and 7.32  
 477  $\times 10^{-5}$  C at 600  $\mu\text{S}/\text{cm}$  respectively. Chloride has a slightly higher charge, and bicarbonate the lowest, with an  
 478 increase in charge with an increase in conductivity. The average charge transferred during electrochemical pulses  
 479 was shown to increase with time, from 6.56e-5 C to 9.56e-5 C. A decrease in solution conductivity from 1200  
 480  $\mu\text{S}/\text{cm}$  to 600  $\mu\text{S}/\text{cm}$  resulted in only a slight decrease in electrochemical pulse charge of ~2%.

481  
 482 To confirm whether gap conditions were crucial to the process, the percentage of high voltage regions were  
 483 measured for each electrolytic-dielectric, for the two conductivity levels. As shown in Figure 11, NaCl showed

484 the highest percentage of high voltage regions; while NaHCO<sub>3</sub> showed the least out of the electrolytic-dielectrics  
 485 (DI is most stable). The difference is small at 600 μS/cm however is clearer at 1200 μS/cm.



486

487 Figure 11. **High voltage zones for electrolytic-dielectrics.** Change in instability percentage for different  
 488 electrolytic-dielectrics at 600 and 1200 μS/cm conductivity

489 **4. Discussion**

490

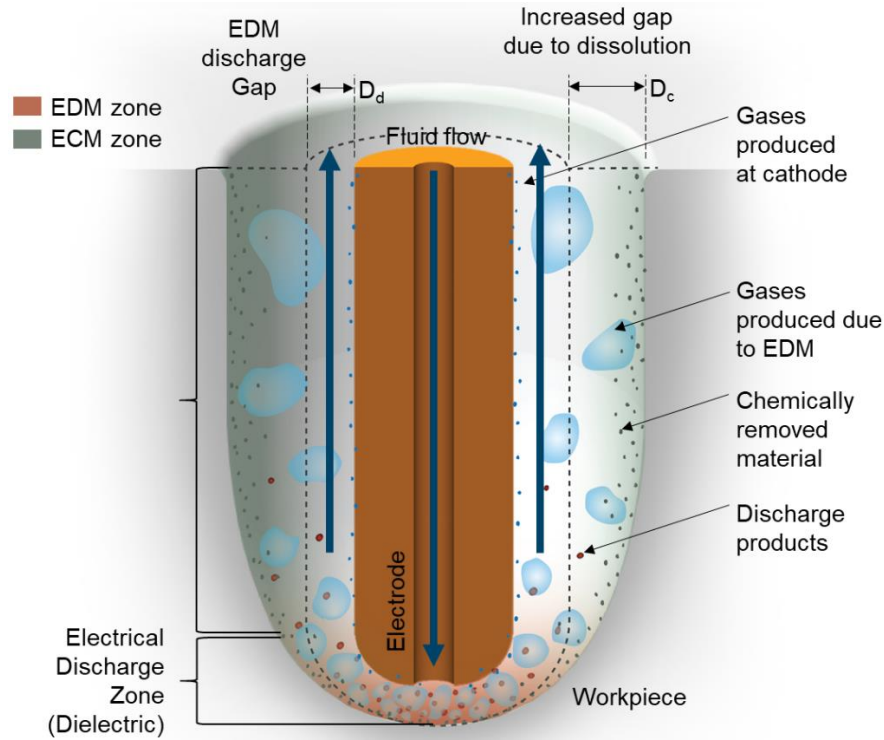
491 4.1. Hybrid Removal Mechanisms

492

493 It is now possible to deduce the working mechanisms of the process. From Figure 3 it was shown that two distinct  
 494 regions on the surface are present, the EDM zone and the ECM zone, separated by a transition area. These zones  
 495 change proportions with increased conductivity, which then reduces the EDM zone.

496 This change in EDM zone can be explain by the macro-scale of the process. When machining starts, the discharge  
 497 gap,  $D_d$  in Figure 12, is equal on the frontal and side areas. This results in electrical discharges throughout the  
 498 entire surface, therefore dominating removal while electrochemical removal is limited. Once the side gap,  $D_c$ ,  
 499 begins to expand larger than the discharge gap, due to simultaneous electrochemical removal, secondary  
 500 discharges [30], and debris bridges, removal at the side walls begins to be dominated by anodic dissolution.  
 501 Although anodic dissolution occurs throughout the entire surface which is exposed to electrolytic dielectric, EDM  
 502 only occurs on the frontal area of the electrode, i.e. where the gap distance is shortest. When a sufficient side gap  
 503 is reached, only electrochemical removal occurs as the gap is so large the likelihood of discharge is effectively

504 reduced to zero. Thus, electrolytic behaviour of the working fluid dominates in this region. The reduced electrical  
 505 discharges on the side walls also results in reduced electrode side wear proportional to the conductivity, resulting  
 506 in reduced electrode frontal curvature due to discharges focussing on the frontal area. The minimum EDM zone  
 507 can therefore is equal to the sum of the corner radius and spark gap, as this region is the area that, in addition to  
 508 the frontal area, advances towards the workpiece material to initiate electrical discharges.



509

510 Figure 12. **Proposed process mechanisms.** EDM and ECM hybrid process showing simultaneous chemical and  
 511 discharge removal. Distinct EDM and ECM zones are present in the process. ECM zones caused due to  
 512 increasing gap, reducing discharges in the regions. Frontal area gap is smaller than EDM discharge gap resulting  
 513 in sparks.

514

515 Therefore, the side area can be considered electrolytic locally, while the frontal area as dielectric. EDM discharges  
 516 are thus used to advance hole depth, while anodic dissolution is used to remove recast layer, simultaneously. In  
 517 this case, the electrochemical side does not significantly affect the EDM side, as shown by the minimal change in  
 518 MRR with conductivity and EDM zone. This may be due to the increase in gases (due to production of cathodic  
 519 hydrogen and anodic oxygen, which increase with conductivity) and so promotes EDM sparking due a decreased  
 520 breakdown strength and preferential discharge paths caused by debris accumulation at bubble interfaces. It may  
 521 also be the case that at the low conductivities used, electrical breakdown is not significantly hindered, therefore  
 522 breakdown still occurs. If the dielectric conductivity is increased by a magnitude, then it can be predicted that  
 523 pulse energy would cause high electrochemical current through the electrolyte which would clearly hinder

524 breakdown. This is the case in ECDM in which current causes electrochemical gas generation instead of a standard  
525 discharge, and the actual discharge only occurs between the boundary of the large gas bubble and electrode. EDM  
526 and anodic dissolution can therefore be considered to occur simultaneously on the macro scale, while on the  
527 individual discharge scale they occur concurrently.

528 The dotted line region in Figure 12 shows electrochemically removed material, while the inverse region of  
529 diameter  $D_d$  shows the material removed via EDM only. This results in a surface characteristic of anodic  
530 dissolution, whilst exhibiting zero discharges on its surface. The red region shows the EDM zone, which is also  
531 the zone with increased temperature. The green zone shows the ECM zone, in which the concentration of ECM  
532 removed material reduces further away from the surface (shown by the gradient).

533 On the microscale, increased anodic dissolution through pitting occurs when conductivity is increased, due to a  
534 higher concentration of aggressive chloride anions (increasing charge passed) reacting with the anode workpiece  
535 surface liberating metallic hydroxides into the fluid. This increase in dissolution is also seen along the axis of  
536 holes due to increased exposure time of the workpiece surface to the anions available in the electrolytic dielectric,  
537 with larger and deeper pits occurring towards the entrance of the hole which coalesce into a smoothed surface.  
538 The decrease in roughness can also be explained by anodic levelling, in which protruding sections of recast are  
539 preferentially removed by the primary current distribution [31], which is intensified with an increase in dielectric  
540 conductivity and exposure time.

541

#### 542 4.2. Surface modification mechanisms

543

544 In the case of chloride anions, anodic dissolution occurs by aggressive electrochemical pitting, which rapidly  
545 removes material [32], either when there is no formed oxide layer or through breakdown of the oxide layer and  
546 increased passage of anions to the exposed metal [33]. Between Fig. 3d–h, the change in pit morphology can be  
547 explained by superposition of pits. As machining time increases the pits increase in diameter and begin to overlap  
548 which cause the holes to merge, resulting in a markedly smoother surface [36]. In addition it is also likely that the  
549 surface is levelled via electrochemical levelling, which occurs when differences in potential between peaks and  
550 valleys results in more removal at peaks. This results in a hole with varying surface morphology along the hole  
551 surface, limiting control on the surface.

552 For  $\text{NaHCO}_3$  the electrochemical effect on the recast layer is notably different. With passivating electrolytes, the  
553 anions (e.g. bicarbonate) react with the base material to produce a protective oxide layer at the metal-liquid

554 interface, which restricts further chemical removal of the metal [7, 31]. Removal may also be through diffusion  
555 control, when the movement of atoms and ions through a viscous, diffusion, or thin oxide film layer, towards the  
556 metal surface, metal-oxide interface, or oxide-liquid interface This oxide layer is seen throughout the surface, as  
557 compared to the concentrated EDM oxides, and is also mechanically weaker as no oxides survived polishing.  
558 During the process, due to the brittle nature cracks and spalling occur due to flushing and temperature gradients.  
559 The bicarbonate ions then react with the exposed metal to remove more of the recast layer. Oxide film breakdown  
560 can also be explained by transpassive dissolution due to the formation of unstable oxides, in which the oxide film  
561 begins to break down, further aiding oxide film spalling, thus enabling further pitting or oxide formation [9]. Other  
562 areas on the surface also exhibit electrochemical removal by mild pitting (compared with chloride). At certain  
563 conditions pitting can occur which leads to a reasonably smooth surface as pits superimpose [7]. This implies that  
564 a cyclic process of passive layer formation, layer removal, pitting, and passive layer reformation occurs throughout  
565 the machining of a hole. The hole also exhibits a consistent surface morphology due to limited electrochemical  
566 removal, thus the electrochemical removal is more controlled, albeit with limited recast removal and generation  
567 of surface oxides.

568 Unlike  $\text{NaHCO}_3$ , for  $\text{NaNO}_3$  the oxide layer is not present on the surface after machining, which may be due to  
569 the increased electrochemical removal compared to oxide formation which results in the oxide layer not building  
570 up and instead being continuously removed (due to the high-pressure flushing, thermal gradients, and pitting).  
571 Localised dissolution may be due to the anodic dissolution generated oxide film breakdown at defect sites such  
572 as pores within the oxide layer, which causes localised breakdown and pitting [34]. Further removal occurs more  
573 easily in these 'activated' areas compared to areas protected by oxide, compounding material removal. Even after  
574 re-formation of the oxide layer in the pitted areas, and the removal of the oxide layer in other areas, the two distinct  
575 regions will remain. Another possible reason for selective electrochemical removal is that anodic dissolution is  
576 reduced on the areas with EDM generated oxides, which usually surround the craters. Thus, dissolution first occurs  
577 on the exposed metal followed by the EDM oxide regions after these oxides have spalled off. This is also seen for  
578  $\text{NaHCO}_3$ , but not for  $\text{NaCl}$  due to breakdown being actively promoted with more breakdown points per unit area,  
579 while for  $\text{NaHCO}_3$  and  $\text{NaNO}_3$  there are fewer breakdown points, which then enlarge. Conversely, in some areas  
580 the EDM generated oxides may spall off first, which then results in dissolution in those areas due to preferential  
581 chemical dissolution. The pits are considerably larger than  $\text{NaCl}$ . This may be due to the hole depth and MRR  
582 being significantly less than  $\text{NaCl}$  (a reduction of 37.7% in MRR from deionised water), due to reduced electrical  
583 discharges, which would increase the time for electrochemical machining on the smaller hole internal surface,

584 compared to the deeper and thus larger area NaCl machined hole. This implies that if there are fewer electrical  
585 discharges occurring per second, which would result in a shallower hole, then anodic dissolution of the recast  
586 layer will increase due to the smaller electrochemical machining area that effectively focuses the current density.  
587 Thus, controlling the amount of electrical discharges is key to controlling the amount of dissolution of the recast  
588 layer. The change in surface morphology is similar NaCl. In addition, controllability is further limited due to  
589 strong localised pitting resulting large pits with some portions of the surface with remaining recast.

590 The nitrite ion from  $\text{NaNO}_2$  is well known to be a passivating corrosion inhibitor which easily forms an effective  
591 oxide film on a surface [27, 35]. Compared to  $\text{NaNO}_3$  it can be assumed that the formed oxide layer is more stable  
592 thus reducing the rate of electrochemical dissolution resulting in a surface which is more uniformly machined  
593 with reduced pitting. This can be explained though the diffusion-controlled removal mechanisms, in which  
594 electrochemical removal is limited due to either a viscous layer, salt layer, or thin oxide film [31]. The surface  
595 morphology is more controlled than  $\text{NaNO}_3$  with no remaining recast regions, however preferential pitting occurs  
596 resulting in areas of excessive electrochemical removal.

597 At  $1200 \mu\text{S}/\text{cm}$   $\text{Na}_2\text{SO}_4$  is significantly levelled with no sign of pitting or oxide layers. This may be due to the  
598 oxide layer formed controlling chemical removal of the base material via controlled diffusion, resulting in a  
599 polished surface. Electrochemical polishing is when atoms are removed through controlled means stochastically  
600 where removal is delocalised from geometry due to thin film oxide layers. Polishing is thus at the micro scale  
601 compared to levelling and is controlled through surface layers. To achieve this, a thin and compact film must form  
602 which is contaminated by significant amounts of anions from the solution while also having sufficient ionic  
603 conductivity to allow for the passage of cations at a high rate [7]. A large portion of the surface has similar  
604 morphology (smoothed) thus can be considered to be a controllable surface with no excessive electrochemical  
605 removal.

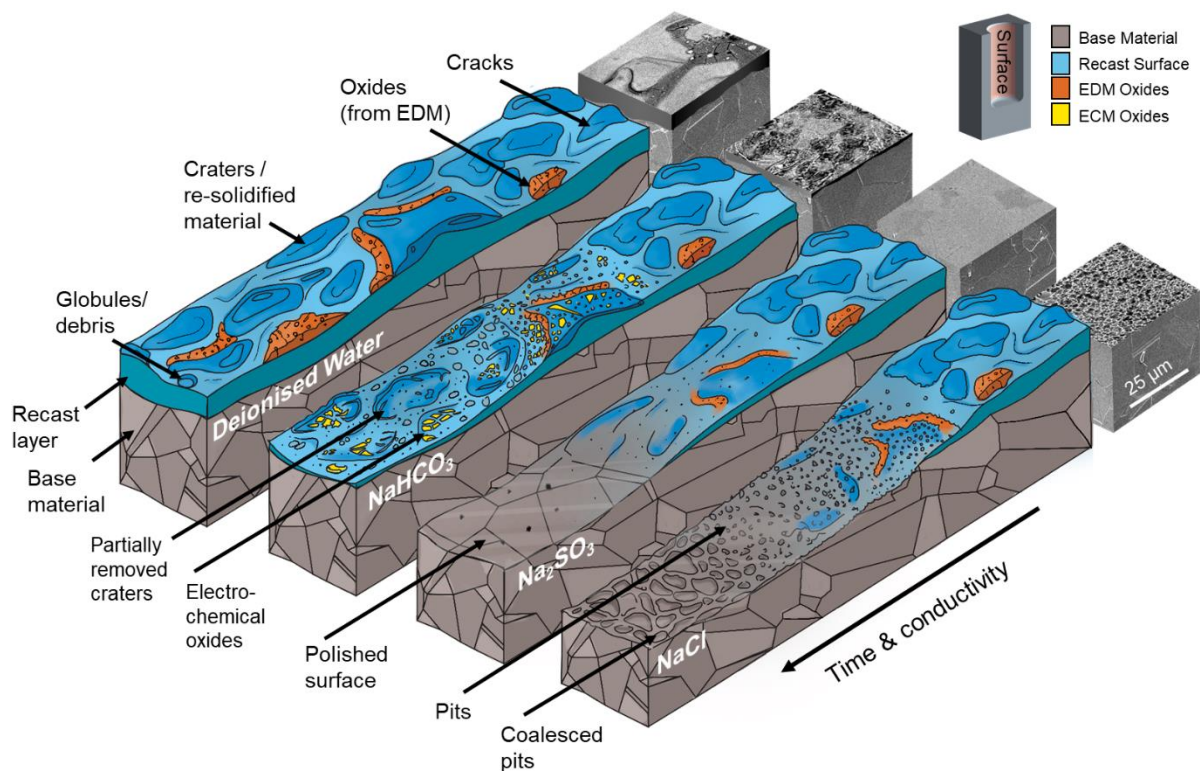
606  $\text{Na}_2\text{SO}_3$  exhibits a finely polished surface showing grain boundaries and little edge removal.  $\text{Na}_2\text{SO}_3$  is a reducing  
607 agent, commonly used as a corrosion inhibitor by the mechanisms of oxygen scavenging which removes dissolved  
608 oxygen from the solution by oxidising to  $\text{Na}_2\text{SO}_4$  [28]. A decrease in oxygen content would then decrease the  
609 acidification of the zone thus reducing the rate of chemical dissolution further, as compared to  $\text{Na}_2\text{SO}_4$ .  $\text{Na}_2\text{SO}_3$   
610 is therefore shown to produce the most favourable surface in terms of surface integrity with no apparent surface  
611 defects at this length scale. A change in surface morphology similar to  $\text{Na}_2\text{SO}_4$  is seen, but with increased  
612 electrochemical removal and leading to a smoother surface.  $\text{Na}_2\text{SO}_3$  can be considered to be the most controllable,  
613 in terms of no excessive electrochemical removal and with a large proportion of the surface exhibiting similar and

614 preferred surface morphology.

615 From Figure 8 it was shown that the EDM zone decreases with conductivity for all electrolytic-dielectrics. This  
616 is due to increased ions available for anodic dissolution. NaCl was shown to have the smallest EDM zone due to  
617 it being the most aggressive additive, followed by  $\text{Na}_2\text{SO}_3$  which was explained to be the least aggressive. A  
618 smaller difference with an increase in conductivity was also shown for  $\text{Na}_2\text{SO}_3$  and  $\text{NaNO}_2$ , as compared to  
619  $\text{Na}_2\text{SO}_3$  and  $\text{NaNO}_3$  respectively. This is also due to these salts being less aggressive due to the differences in  
620 chemical dissolution mechanisms as discussed previously (effect corrosion inhibition for  $\text{NaNO}_2$  and oxygen  
621 scavenging for  $\text{Na}_2\text{SO}_3$ ).

622

623



624

625 **Figure 13. Altered surfaces through different chemical mechanisms.** Showing the different surface  
626 morphologies due to three different types of chemical effects on the recast layer. SEM images of each surface to  
627 relate illustration to machined hole surfaces.

628 The electrochemical part of the process can thus be generalised into three discrete mechanisms - oxide-limited  
629 passive removal, electropolishing, and aggressive removal, as shown in Fig. 13 with  $\text{NaHCO}_3$ ,  $\text{Na}_2\text{SO}_3$ , and  $\text{NaCl}$ ,  
630 respectively. DI shows a typical EDM recast layer with surface defects.  $\text{NaHCO}_3$  shows a surface with limited  
631 electrochemical removal and the presence of electrochemically induced oxides. Here electrochemical removal is  
632 limited due to energy (charge) being used in production of surface oxides instead of removing recast layer

633 material, resulting in gradual but limited removal. In electrochemical machining, gas is generated from the cathode  
634 via hydrogen evolution. Oxygen can also be generated on the anode surface, which is promoted when oxide layers  
635 are present [9]. For  $\text{NaHCO}_3$  it can be assumed that gas generation is high due to the oxide layers formed on the  
636 surface, while for  $\text{Na}_2\text{SO}_3$  gas generation may be low due to no presence of oxides. More energy is thus used for  
637  $\text{NaHCO}_3$  instead of removing material compared to  $\text{Na}_2\text{SO}_3$ , resulting in a lower current efficiency. The second  
638 mechanism combines electrical discharges with electropolishing. Here the recast layer is removed gently through  
639 diffusion-controlled means, resulting in a surface with little pitting with most of the recast layer removed. This  
640 may be through a compact thin film or viscous salt layer.  $\text{Na}_2\text{SO}_4$  is shown to gently remove material with some  
641 pitting which shows breakdown of the layer, while  $\text{Na}_2\text{SO}_3$  gently removes the recast layer with minimal pitting,  
642 leading to a smooth and controlled surface with no pitting.  $\text{SO}_3^{2-}$  is also an oxygen scavenger which removes  
643 dissolved oxygen from the solution by oxidizing to  $\text{SO}_4^{2-}$  [28]. This might alter the pH of the machining zone,  
644 leading to slow and controlled dissolution resulting in a polished surface. The third mechanism involves  
645 aggressive pitting, and these pits grow in size with time and increased conductivity, ultimately coalescing into a  
646 smooth, yet pitted surface.

647  $\text{NaCl}$  is shown to remove material via aggressive pitting which lead to pit superimposition.  $\text{NaNO}_3$  and  $\text{NaNO}_2$   
648 show surfaces with a mixture of electro-polishing and pitting.  $\text{NaNO}_3$  removes material by pitting in some areas,  
649 while having limited removal in some, leading to a mostly pitted surface with spots of remaining recast.  $\text{NaNO}_2$   
650 shows a surface with minimal pitting, leading to a smooth surface with large pits at preferential areas.

651 It was shown that hole accuracy was influenced by the electrolytic-dielectrics in terms of affecting the overcut.  
652 Electrolytic-dielectrics with increased electrochemical removal, such as  $\text{NaCl}$  and higher conductivities, will  
653 remove more material on the sidewalls in addition to the EDM overcut, therefore potentially negatively affecting  
654 hole accuracy. Compared to DI, which had a 4.6 % overcut,  $\text{NaCl}$  at 1200  $\mu\text{S}/\text{cm}$  produced the lowest accuracy  
655 with a 8.4 % overcut. However,  $\text{Na}_2\text{SO}_4$ , which was shown to be least aggressive and most controllable salt,  
656 produced an overcut of only 5.2 % at 1200  $\mu\text{S}/\text{cm}$ , an increase of only 1.4 % overcut compared to DI. This small  
657 increase in overcut and decrease in MRR is a fair compromise for a surface with no recast, and can easily be  
658 addressed through improvements to process control, process optimisation, and electrolytic-dielectric composition  
659 which will be discussion in Chapter 4.3 and in future work.

660

661 4.3. Elucidating Pulse Behaviour

662

663 Through capturing waveforms, it was shown that distinct pulse types are present. The most important pulse type  
664 in this process is the high voltage/electrochemical pulse as this is the pulse that drives electrochemical dissolution  
665 of the EDM recast layer. This pulse type occurs in regions where a high voltage is observed. Though in DI this  
666 high voltage causes near-zero current to flow, when conductivity is increased, by addition of ions, a current can  
667 flow causing electrochemical machining. The current flow in the off-time can be explained due to the capacitance  
668 in the system. The capacitance is likely caused by the charging of the electric double layer. The electric double  
669 layer is formed when the charged anode attracts oppositely charged ions forming two layers, one of which is the  
670 compact oppositely charged layer and the other is the diffuse layer in which the concentration decreases further  
671 from the anode surface. In the on-time this capacitive layer is charged and subsequently discharged in the off-time  
672 [8]. Therefore, the regions of high voltage are crucial in controlling the dissolution process.

673 These high voltage regions normally occur when dielectric breakdown cannot occur due to a large IEG [36]. This  
674 may be at the instance when the electrode is advancing towards the workpiece to initiate voltage breakdown, when  
675 enough material is removed that the gap is too large, or when the electrode is retracted due to unfavourable gap  
676 conditions (as in leading to arcing or short circuits). High voltage instances can also occur as discharge delay  
677 regions, which occur at the start of delayed pulses. These delayed regions occur also due to too large IEGs, but  
678 can also be significantly affected by factors that can alter the local dielectric strength such as fluid dielectric  
679 constant, open voltage, gas volume, temperature, electrode workpiece geometry, and contaminants/debris.

680 Through waveform analysis, it was observed that the majority of the electrochemical pulses were grouped together  
681 in packets, with a small number interspaced between electrical discharge or semi-arc pulses ( $< 1\%$ ). Discharge  
682 delayed pulses, which have a portion of electrochemical machining at the start of the pulse, only accounted for 1  
683 % to 2.5 % of pulses. Therefore, it can be assumed that the main driver of electrochemical removal are the pulses  
684 which occur in large packets. These regions can be inferred to correlate to the instances of electrode retraction  
685 due to gap conditions (inability to cause breakdown). In this case, the pulse energy due to the high voltage causes  
686 electrochemical dissolution as opposed to an electrical discharge. Whether the energy causes ECM or EDM  
687 therefore depends on gap conditions and is the basis for the need to control pulse ratio.

688 The EDM zone, as shown in Fig. 12, is the zone where EDM discharges occur. Due to the smaller IEG and  
689 increased gas and debris in the region, this zone locally acts as a dielectric causing electrical breakdown. This  
690 explains why EDM discharges are identical between conductivities. However, in regions of high voltage no  
691 breakdown occurs thus the region acts as an electrolyte. The balance between EDM and ECM discharges therefore  
692 is heavily influenced by gap conditions, which are affected by EDM parameters as well as dielectric and salt

693 additives. By controlling the amount of EDM pulses the dissolution of the recast layer can also be controlled.

694

695 The influence of gap conditions on the process was shown in Figure 11. NaCl showed the most high voltage  
696 zones, followed by  $\text{Na}_2\text{SO}_3$ ,  $\text{NaHCO}_3$ , and DI, with the difference being more clear at  $1200 \mu\text{S}/\text{cm}$ . The increase  
697 in conductivity was shown to increase the high voltage zones for all electrolytic-dielectrics, showing that the cause  
698 of the high voltage zones and instability is electrochemical machining. This may be due to the increased anions,  
699 which cause a charge to be transferred and thus hinders electrical discharges. This can also be explained by the  
700 electrochemical charge causing the EDM gap to increase due to flowing current, therefore increasing machining  
701 voltage and also increasing likelihood of high voltage zones due to the enlarged gap [37]. With depth the average  
702 electrochemical pulse charge increased from  $6.56\text{e-}5 \text{ C}$  to  $9.56\text{e-}5 \text{ C}$ , possibly due to the increased ions, area,  
703 stored charge, or conductivity, which subsequently results in the increase in high voltage zones. If the current flow  
704 or charge being stored is too large it can also reduce electrode advance due to essentially tricking the EDM pulse  
705 controller into thinking that a discharge is happening due to detected current and voltage values. NaCl shows the  
706 largest high voltage zone percentage, which implies the electrochemical machining it causes has the largest effect  
707 on the gap. This is confirmed by the waveform pulse analysis which showed that pulse charge for NaCl was the  
708 largest, followed by  $\text{Na}_2\text{SO}_3$ , and  $\text{NaHCO}_3$ . Each salt additive is likely to also cause different gap conditions in  
709 both the ECM and EDM zones, such as different volumes of gas, altered surfaces which can affect discharges,  
710 and different types of debris (ECM oxide spalling and size of debris or sludge due to dissolution), which would  
711 then result in different amounts of high voltage regions.

712 While changing the salt additive mainly affects dissolution mechanisms and resulting surface quality, it also  
713 affects the amount of EDM and ECM pulses. The effect of these high voltage zones can be seen in the waveform  
714 pulse analysis which categorises each individual pulse into types. NaCl has the most ECM pulses, with  $\text{NaHCO}_3$   
715 has the least. For both NaCl and  $\text{Na}_2\text{SO}_3$  a large decrease in EDM pulses is seen at 20 seconds, however an increase  
716 is seen till 35 seconds.  $\text{NaHCO}_3$  shows a linear decrease which may be due to limited electrochemical removal  
717 due to oxide layer restrictions. At  $600 \mu\text{S}/\text{cm}$  there are more EDM discharges and the increase in electrochemical  
718 pulses is less steep indicating limited anodic dissolution due to reduced ions for anodic dissolution, and so a  
719 limited influence on electrical breakdown in the EDM zone. The EDM pulse ratio also decreases with time and  
720 depth, resulting in increased electrochemical pulses and decreased electrical discharges, linking an increase in  
721 high voltage regions with increased electrochemical pulses. The pulse ratio results are reflected in the high voltage  
722 zone trends, showing that both are directly linked. The increase in high voltage zone thus results in more ECM

723 pulse types and a reduction in EDM pulses. Therefore, the percentage of high voltage zones is a more efficient  
724 way to measure and control the balance between the EDM and ECM sides of the process. The results also  
725 confirmed that the electrochemical pulses scattered throughout machining can be essentially ignored, in favour of  
726 the electrochemical pulses in the instability regions of high voltage. Thus, this is a better measure for EDM ECM  
727 balance and a method to control anodic dissolution of the recast layer.

728

#### 729 4.4. Enhancing understanding through process modelling

730 To understand the process balance between the electrical-discharge and electrochemical aspects of the process,  
731 and the influence of altered dielectrics, a process model was needed. ECM pulse data is needed to simulate  
732 electrochemical removal, while EDM process data is needed to simulate hole advance. The theoretical zero recast  
733 point can thus be calculated, and with a current efficiency this point can be corrected. Thus, the model can help  
734 illustrate the importance of balancing the EDM to ECM pulse ratio to achieve a desired surface.

735 Current-time values were obtained from Section 3.4 in which pulse analysis was used to obtain average charge  
736 and pulse data, for electrochemical pulses observed in the process.

737

738 In order to model the process it was assumed that the direct interactions between electrical discharges and  
739 electrochemical machining were negligible i.e. electrical discharges are solely used to advance hole depth and  
740 create the EDM overcut, while electrochemical discharges are solely used to remove material from the recast layer  
741 (normal to the direction of hole advance). The EDM material removal can be modelled by using the MRR from  
742 machining with DI, while the electrochemical material removal can be modelled by Faradays Law in Equation  
743 (1).

744

$$745 \quad m = \frac{1}{F} \left( \frac{M}{v} \right) \int_{t_0}^{t_f} I \, dt = ZQ \quad (1)$$

746

747  $m$  is the mass removed by electrochemical removal,  $F$  is Faradays number,  $M$  is molar mass,  $v$  is ion valency,  $I$  is  
748 current, and  $t_0$  and  $t_f$  are the time limits over which the current time integral is taken. The equation can be simplified  
749 further where  $Z$  is the electrochemical equivalent of the material Table 1, and  $Q$  is the charge passed.

750 The recast layer/workpiece depth removed can then be calculated by Equation (2) which converts the mass to a  
751 volume removed from the sidewalls, and then to a recast depth removed.  $Y$  is the recast depth removed,  $h$  is the  
752 depth over which the volume is removed,  $\rho$  is the density of the metal, and  $D_1$  is the total diameter of the electrode

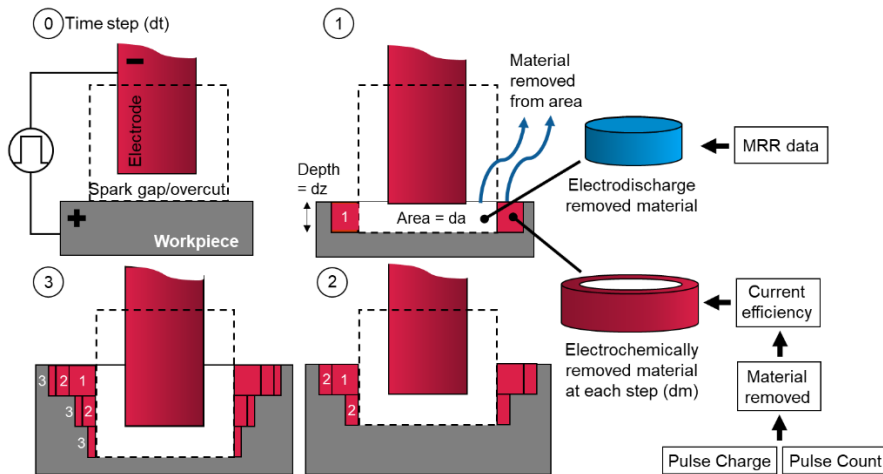
753 and EDM overcut.

754

755 
$$y = \frac{1}{2} \left( \sqrt{\frac{4m}{\pi h \rho} + D_1^2} - D_1 \right) \quad (2)$$

756

757 Fig. 14 shows that after one time step, two volumes of material are removed. The EDM removed material depends  
758 on the MRR, and is the area through which the electrode and spark gap/overcut removes material through the  
759 workpiece, in one time step. At the same time the electrochemically removed material, calculated by Equation  
760 (1), is removed from the recast layer. The amount of electrochemically removed material is calculated using the  
761 current-time values obtained previously in which pulse analysis was used to obtain average charge and pulses per  
762 second data, for electrochemical pulses observed in the process. After each step the area increases, however the  
763 ECM removed material per pulse remains the same resulting in the removal over a larger area. This concentrates  
764 the removal in areas which are machined for more time.



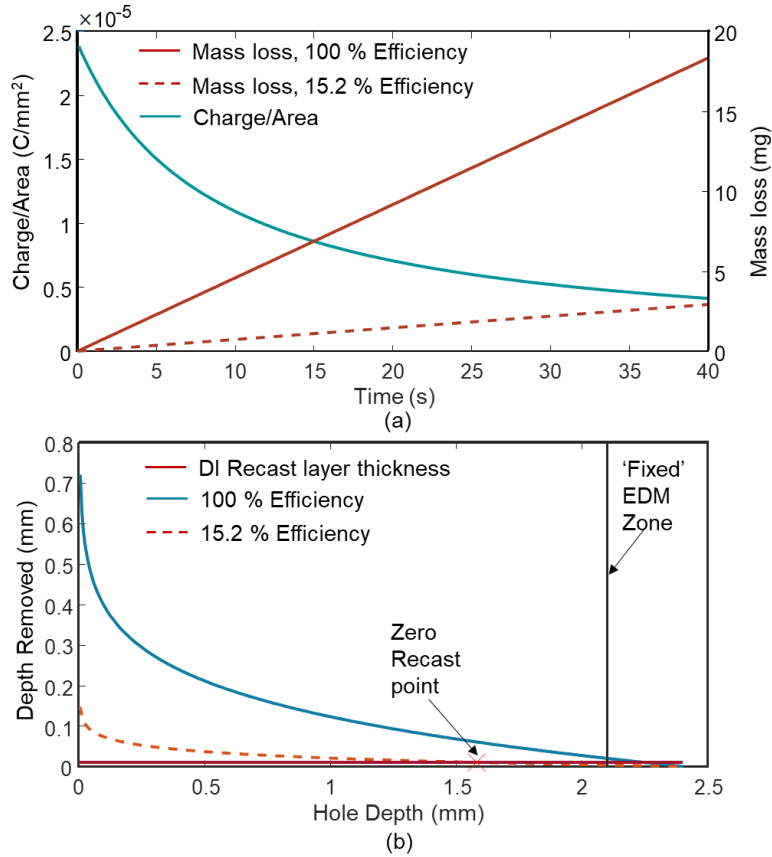
765

766 Figure 14. **Process model explanation.** Showing 4 time steps and resulting material removal

767 While Equation (1) calculates the material removed due to electrochemical machining, it does not account for the  
768 energy not used to removed material, such as in the generation of gas and oxides [38]. To account for this a current  
769 efficiency is needed to correct the calculated mass removed, which was calculated by drilling a hole with DI  
770 producing an EDM recast layer, then machining this with pure electrochemical machining with the same process  
771 conditions used in this paper.

772 The current efficiency was estimated as 15.2 % using sulfite, and Fig. 15 shows the results of the model. Fig. 15a  
773 shows the change in charge per area as the hole advances. The area increases as depth advances which reduces  
774 the amount of charge on an individual area, resulting in the expected hole geometry. Fig. 15b shows the amount

775 of recast depth removed and essentially shows the resulting hole profile. The current efficiency has a large  
 776 influence on the resulting profile, however it is a more accurate representation of real machining.  
 777



778  
 779 Figure 15. **Results of model.** a) Change in Charge per Area and mass loss with time, at 1200  $\mu$ S/cm. b) Amount  
 780 of recast depth removed with depth, showing the zero recast point, fixed EDM zone, and affect of current  
 781 efficiency on the model.

782  
 783 One factor not considered in the model was the influence of gap distance on gap resistance and the influence on  
 784 electrochemical machining. Although from Fig. 15b it shows considerably more material is removed between 0  
 785 and 0.5 mm compared to 0.5 mm to the end, in a real example this difference is less pronounced due to reduced  
 786 material removal at areas of increased gap distance. This relationship can be described by Equation (3) in which  
 787 an increase in gap distance increases resistance along the path. This resistance ultimately reduces electrochemical  
 788 material removal at areas of high resistance. Although the total material removed will be the same, the distribution  
 789 will differ. The end result of this will be that the predicted zero-recast point will be further down the hole.

790  
 791

$$R = \frac{V}{I} = \frac{y}{Ak} \quad (3)$$

792

793 Fig. 15b also shows a fixed EDM discharge zone. This zone is entirely influenced by the electrode corner wear.

794 Although in this model no electrode wear was assumed, in reality corner wear will occur. This will result in a

795 fixed EDM zone that is equal to the sum of the corner radius and spark gap, as this region is the area that, in

796 addition to the frontal area, advances towards the workpiece material to initiate electrical discharges.

797 Fig. 16 shows the differences in recast layer removed between salts.  $\text{NaHCO}_3$  has the largest EDM discharge

798 zone, while  $\text{NaCl}$  has the lowest, which is related to the differences in pulse charge and amount, while the hole

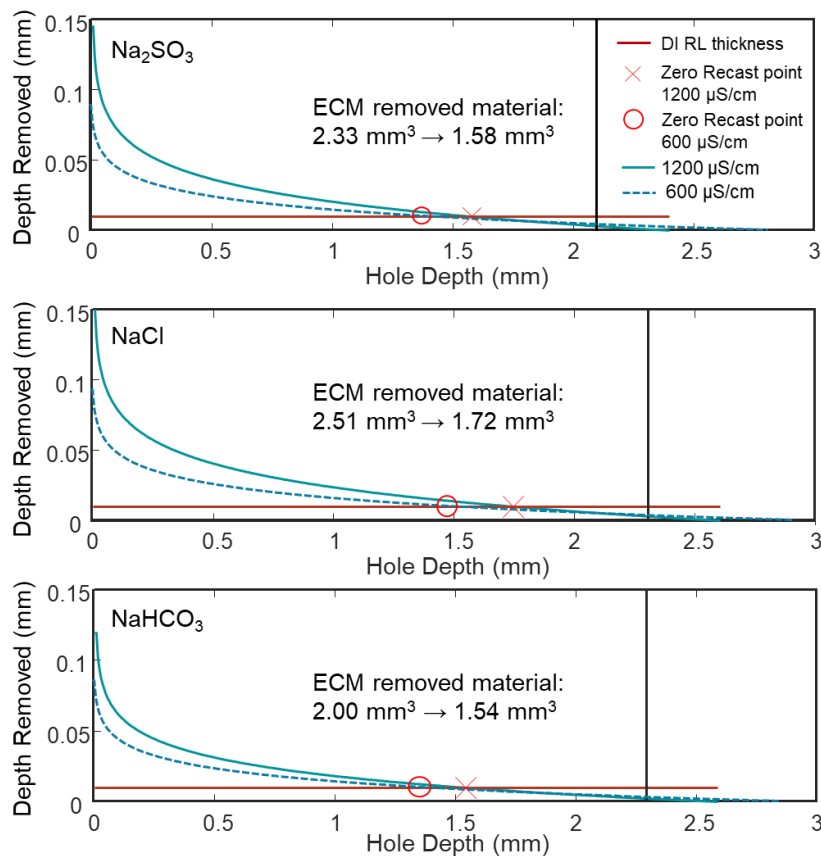
799 depth is related to MRR. Largest ECM removed material is seen for  $\text{NaCl}$ , and the lowest for  $\text{Na}_2\text{SO}_3$ . The zero

800 recast point also shifts down the hole when conductivity is increased due to the increased electrochemical

801 machining, with the largest change seen for  $\text{NaCl}$ . Although the expected trend is seen, the difference would be

802 considerably larger if current efficiency was calculated for each salt, as the differing electrochemical mechanisms

803 would result in different anodic efficiencies.



804

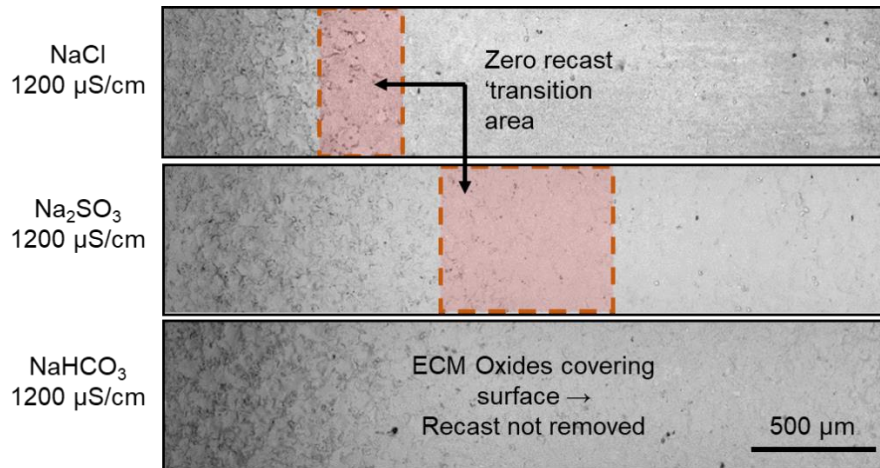
805 Figure 16. **Modelled recast layer profile.** Shows resulting model hole profile for the electrolytic-dielectrics

806 based on pulse data captured at the calculated current efficiency. A zero-recast point is shown for each profile at

807 two conductivity levels with the amount of ECM removed material.

808

809 The zero recast point was measured as a range, from the optical and SEM surface images, and confirmed with  
 810 recast layer cross sections. An example of the difference in zero recast layer zones is shown in Fig. 17, and the  
 811 values shown in Table 2. Comparatively, the three dielectrics and conductivities behave similarly as modelled,  
 812 that is NaCl has the lowest zero recast point followed by Na<sub>2</sub>SO<sub>3</sub>, and an increase in conductivity pushes the zero  
 813 recast point further down.  
 814



815  
 816  
 817 **Figure 17. Example differences in zero recast zones for three dielectrics.** The zero-recast transition area is  
 818 highlighted in red, and is the area where zero recast occurs. NaHCO<sub>3</sub> shows no zero recast area due to surface  
 819 oxides.

820  
 821 However, NaHCO<sub>3</sub> exhibits a surface which never reaches zero recast due to oxide formation due to ECM. The  
 822 material removed in the model does not include the oxidation reaction, as in reality the material is mostly oxidised  
 823 and remains on the surface with some spalling. The oxidation reaction is not included in the model. NaCl also  
 824 shows zero recast points further down than modelled. This can be explained by the current efficiency being  
 825 considerably higher for NaCl due to it being an aggressive salt (through active dissolution) as compared to the  
 826 other dielectrics. This factor was not included in the model as the current efficiency was calculated using one  
 827 dielectric (Na<sub>2</sub>SO<sub>3</sub>). The difference in current efficiency for different electrolytic-dielectrics can be used as a way  
 828 to encapsulate the various influences on the ECM side of the process as an easily applied corrective factor.  
 829 Although gap conditions won't be the same due to hole advance and EDM gases and debris, it is a good method  
 830 to characterise different electrolytic-dielectrics for use in selection and should be considered for future work.

831  
 832 **Table 2- Zero recast point ranges for machined holes compared to the model.** Ranges calculated from 3  
 833 holes.

<b>Dielectric</b>	<b>Zero recast point (mm)</b>	
	<b>Model</b>	<b>Experiment</b>
<b>NaCl 600 <math>\mu\text{S/cm}</math></b>	1.47	1.61 – 2.01
<b>NaCl 1200 <math>\mu\text{S/cm}</math></b>	1.74	1.72 – 2.12
<b>NaHCO<sub>3</sub> 600 <math>\mu\text{S/cm}</math></b>	1.34	-
<b>NaHCO<sub>3</sub> 1200 <math>\mu\text{S/cm}</math></b>	1.53	-
<b>Na<sub>2</sub>SO<sub>3</sub> 600 <math>\mu\text{S/cm}</math></b>	1.38	0.65 – 0.93
<b>Na<sub>2</sub>SO<sub>3</sub> 1200 <math>\mu\text{S/cm}</math></b>	1.58	0.82 – 1.40

835

836 By altering the electrolytic-dielectric through the choice of salt additives and therefore conductivity, the resulting  
837 hole profile, accuracy, and zero recast point can be controlled, as well as the resulting surface integrity. Similarly,  
838 by altering the pulse charge and frequency for ECM and EDM pulses throughout machining of the hole the recast  
839 layer and process can also be fine-tuned. This ‘pivot-point’ mechanism between EDM and ECM and the resulting  
840 zero-recast point is crucial to producing a tailored surface and should be explored further through altering of EDM  
841 parameters. Process optimisation can then be used to achieve desired hole surface morphology and accuracy,  
842 through the understanding gained through this work. This process adaptation and its fundamental understanding  
843 have significant implications for implementing electrolytic-dielectrics in current EDM setups in high value  
844 applications, where varying hole depths as well as predictable and good mechanical properties are required.

845

## 846 **Conclusions**

847 The proposed hybrid EDM ECM method utilising electrolytic-dielectrics can be a valuable process in high value  
848 manufacturing due to its low cost and ease of machine adaption, combining the accuracy of EDM with the surface  
849 integrity of ECM. The process understanding and theory proposed in this study open up a route to zero recast  
850 machining through control of process fundamentals and key process parameters, which has not been explored  
851 previously. The notion of control of resulting surfaces through tailored electrolytic-dielectrics was shown and is  
852 key to future control of the surface, as well as the idea that the balance of EDM and ECM, which is elucidated  
853 through the EDM:ECM pulse ratio, is critical to producing a tailored and desired surface. Further control of the  
854 process is envisioned through control of EDM parameters to fine tune pulse energies and characteristics, as well  
855 direct control of the pulse ratio. The major conclusions of the study are as follows:

856 • A simultaneous electrical-discharge/electrochemical machining method was developed, which enables a  
857 balance of conventional EDM discharges and anodic dissolution removal of material. This was developed by  
858 increasing the conductivity of conventional deionised water dielectric using dissolution of salts resulting in  
859 electrolytic-dielectrics. An Inconel 718 substrate was used for all tests.

860 • This new process was capable of machining holes successfully, without a significant sacrifice in material  
861 removal rate. Critically, the process can yield a machined surfaces with recast layer entirely removed.

862 • Electrochemical dissolution mechanisms were altered by adding salts which result in distinct removal  
863 processes. Aggressive removal results in a level surface with harsh pitting. Oxide limited passive removal results  
864 in a surface with limited recast removal covered in ECM generated oxides. Electropolishing results in a surface  
865 with a gently removed recast which can be considered metallurgically ideal.

866 Waveform analysis was used to understand pulse types and the balance of EDM to ECM pulses. The process was  
867 split into four pulse types: electrical, semi-arc, delayed, and electrochemical. It was explained that ECM pulse  
868 types are dependent on gap conditions and only occur when EDM pulses cannot, thus controlling EDM to ECM  
869 ratio is key to controlling the resulting surface. The difference between electrolytic-dielectrics was also shown  
870 through the pulse ratio revealing that more aggressive electrolytic-dielectrics have increased ECM pulses. The  
871 time-varying nature of the EDM:ECM balance was also shown to significantly affect resulting surfaces.

872 • A mathematical model was used to illustrate the overall process balance through fundamental  
873 electrochemical theory and process pulse data, adjusted for current efficiency based upon experimental  
874 verification. Through this model, the point during machining at which complete recast layer removal occurs is  
875 predicted and validated through experimental analysis for different salt types, and discrepancies between model  
876 and real data were explained through fundamental EDM/ECM theory.

877 • By altering the electrolytic-dielectric through the choice of salt additives and therefore conductivity, the  
878 resulting hole profile, zero recast point, and expected surface integrity can be controlled. Similarly, by altering  
879 the pulse charge and frequency for ECM and EDM pulses throughout machining of the hole the recast layer can  
880 also be fine-tuned. This 'pivot-point' mechanism between EDM and ECM and the resulting zero-recast point is  
881 crucial to producing a tailored surface.

882 • This adapted process which uses a simple and easily implementable salt dissolution method in a  
883 conventional dielectric, has significant potential to be exploited for producing high-value machined surfaces,  
884 without a mechanically detrimental recast layer. The recast layers on such high-aspect ratio holes cannot be  
885 removed through any reasonable current technology, and therefore use of electrolytic-dielectrics can potentially

886 bypass this expensive addition to the process chain.

887

888 References

889

- 890 1. Kliuev, M., et al., *EDM Drilling and Shaping of Cooling Holes in Inconel 718 Turbine*  
891 *Blades*. Procedia CIRP, 2016. **42**: p. 322-327.
- 892 2. Holmberg, J., A. Wretland, and J. Berglund, *Grit Blasting for Removal of Recast*  
893 *Layer from EDM Process on Inconel 718 Shaft: An Evaluation of Surface Integrity*.  
894 *Journal of Materials Engineering and Performance*, 2016. **25**(12): p. 5540-5550.
- 895 3. Qu, J., et al., *Abrasive micro-blasting to improve surface integrity of electrical*  
896 *discharge machined WC–Co composite*. *Journal of Materials Processing Technology*,  
897 2005. **166**(3): p. 440-448.
- 898 4. Khangura, S.S., et al., *Investigations Into the Removal of EDM Recast Layer With*  
899 *Magnetic Abrasive Machining*, in *ASME 2015 International Manufacturing Science*  
900 *and Engineering Conference*. 2015.
- 901 5. Yan, B.-H., et al., *Improving Electrical Discharge Machined Surfaces Using Magnetic*  
902 *Abrasive Finishing*. *Machining Science and Technology*, 2004. **8**(1): p. 103-118.
- 903 6. Holmberg, J., et al., *Surface integrity after post processing of EDM processed*  
904 *Inconel 718 shaft*. *The International Journal of Advanced Manufacturing*  
905 *Technology*, 2018. **95**(5-8): p. 2325-2337.
- 906 7. Landolt, D., *Fundamental aspects of electropolishing*. *Electrochimica Acta*, 1987.  
907 **32**(1): p. 1-11.
- 908 8. Joshi, S.S. and D. Marla, *11.15 - Electrochemical Micromachining*, in  
909 *Comprehensive Materials Processing*, S. Hashmi, et al., Editors. 2014, Elsevier:  
910 Oxford. p. 373-403.
- 911 9. Lohrengel, M.M., K.P. Rataj, and T. Munninghoff, *Electrochemical Machining—*  
912 *mechanisms of anodic dissolution*. *Electrochimica Acta*, 2016. **201**: p. 348-353.
- 913 10. Wang, C.-C., et al., *Recast layer removal after electrical discharge machining via*  
914 *Taguchi analysis: A feasibility study*. *Journal of Materials Processing Technology*,  
915 2009. **209**(8): p. 4134-4140.
- 916 11. Ramasawmy, H. and L. Blunt, *3D surface topography assessment of the effect of*  
917 *different electrolytes during electrochemical polishing of EDM surfaces*.  
918 *International Journal of Machine Tools and Manufacture*, 2002. **42**(5): p. 567-574.
- 919 12. Wu, X., et al., *Using WECM to remove the recast layer and reduce the surface*  
920 *roughness of WEDM surface*. *Journal of Materials Processing Technology*, 2019.  
921 **268**: p. 140-148.
- 922 13. Kishi, R. and J. Yan, *Electrical Discharge/Electrochemical Hybrid Machining Based*  
923 *on the Same Machine and Tool Electrode*. *Journal of Micro and Nano-Manufacturing*,  
924 2020. **8**(1).
- 925 14. Liu, J.W., T.M. Yue, and Z.N. Guo, *An analysis of the discharge mechanism in*  
926 *electrochemical discharge machining of particulate reinforced metal matrix*  
927 *composites*. *International Journal of Machine Tools and Manufacture*, 2010. **50**(1):  
928 p. 86-96.
- 929 15. Goud, M., A.K. Sharma, and C. Jawalkar, *A review on material removal mechanism*  
930 *in electrochemical discharge machining (ECDM) and possibilities to enhance the*  
931 *material removal rate*. *Precision Engineering*, 2016. **45**: p. 1-17.
- 932 16. Wüthrich, R. and V. Fascio, *Machining of non-conducting materials using*  
933 *electrochemical discharge phenomenon—an overview*. *International Journal of*  
934 *Machine Tools and Manufacture*, 2005. **45**(9): p. 1095-1108.
- 935 17. Krötz, H. and K. Wegener, *Sparc assisted electrochemical machining: a novel*  
936 *possibility for microdrilling into electrical conductive materials using the*  
937 *electrochemical discharge phenomenon*. *The International Journal of Advanced*  
938 *Manufacturing Technology*, 2015. **79**(9): p. 1633-1643.

- 939 18. Zhang, C., et al., *Effect of solution conductivity on tool electrode wear in*  
940 *electrochemical discharge drilling of nickel-based alloy*. The International Journal  
941 of Advanced Manufacturing Technology, 2019. **103**(1): p. 743-756.
- 942 19. Zhang, C., et al., *Surface integrity of holes machined by electrochemical discharge*  
943 *drilling method*. CIRP Journal of Manufacturing Science and Technology, 2020. **31**:  
944 p. 643-651.
- 945 20. Zhang, J., Z. Xu, and C. Zhang, *Variable-parameter high-precision electrochemical*  
946 *discharge drilling method for 440C-Nb without recast layer*. The International  
947 Journal of Advanced Manufacturing Technology, 2020. **110**(9): p. 2815-2826.
- 948 21. Sugahara, T., et al., *Creep Behavior of the Inconel 718 Superalloy*. Defect and  
949 Diffusion Forum, 2012. **326-328**: p. 509-514.
- 950 22. Greene, G.A. and C.C. Finfrock, *Oxidation of Inconel 718 in Air at High*  
951 *Temperatures*. Oxidation of Metals, 2001. **55**(5): p. 505-521.
- 952 23. Jiang, Y., et al., *Adaptive control for small-hole EDM process with wavelet transform*  
953 *detecting method*. Journal of Mechanical Science and Technology, 2012. **26**(6): p.  
954 1885-1890.
- 955 24. Graps, A., *An Introduction to Wavelets*. IEEE Computational Science and  
956 Engineering, 1995. **2**(2).
- 957 25. Yahyavi Zanjani, M., et al., *Process Control in Jet Electrochemical Machining of*  
958 *Stainless Steel through Inline Metrology of Current Density*. Micromachines, 2019.  
959 **10**(4): p. 261.
- 960 26. Speidel, A., et al., *Post processing of additively manufactured parts using*  
961 *electrochemical jet machining*. Materials Letters, 2021. **292**: p. 129671.
- 962 27. Rizvi, M., et al., *Sodium nitrite as a corrosion inhibitor of copper in simulated*  
963 *cooling water*. Scientific Reports, 2021. **11**(1): p. 8353.
- 964 28. Rashid, K.H. and A.A. Khadom, *Sodium sulfite as an oxygen scavenger for the*  
965 *corrosion control of mild steel in petroleum refinery wastewater: optimization,*  
966 *mathematical modeling, surface morphology and reaction kinetics studies*. Reaction  
967 Kinetics, Mechanisms and Catalysis, 2020. **129**(2): p. 1027-1046.
- 968 29. Li, G., W. Natsu, and Z. Yu, *Elucidation of the mechanism of the deteriorating*  
969 *interelectrode environment in micro EDM drilling*. International Journal of Machine  
970 Tools and Manufacture, 2021. **167**: p. 103747.
- 971 30. Murray, J., D. Zdebski, and A.T. Clare, *Workpiece debris deposition on tool*  
972 *electrodes and secondary discharge phenomena in micro-EDM*. Journal of Materials  
973 Processing Technology, 2012. **212**(7): p. 1537-1547.
- 974 31. Han, W. and F. Fang, *Fundamental aspects and recent developments in*  
975 *electropolishing*. International Journal of Machine Tools and Manufacture, 2019.  
976 **139**: p. 1-23.
- 977 32. Frankel, G.S., *Pitting Corrosion of Metals: A Review of the Critical Factors*. Journal  
978 of The Electrochemical Society, 1998. **145**(6): p. 2186-2198.
- 979 33. Datta, M. and D. Landolt, *Film Breakdown on Nickel under Transpassive Dissolution*  
980 *Conditions in Sodium Nitrate Solutions*. Journal of The Electrochemical Society,  
981 1977. **124**(4): p. 483-489.
- 982 34. Wang, D., et al., *Investigation of the electrochemical dissolution behavior of Inconel*  
983 *718 and 304 stainless steel at low current density in NaNO<sub>3</sub> solution*. Electrochimica  
984 Acta, 2015. **156**: p. 301-307.
- 985 35. Chun, K.H., S.H. Kim, and E.S. Lee, *Analysis of the relationship between electrolyte*  
986 *characteristics and electrochemical machinability in PECM on invar (Fe-Ni) fine*  
987 *sheet*. The International Journal of Advanced Manufacturing Technology, 2016.  
988 **87**(9): p. 3009-3017.
- 989 36. Zhang, X., et al., *Intelligent pulse analysis of high-speed electrical discharge*  
990 *machining using different RNNs*. Journal of Intelligent Manufacturing, 2020. **31**(4):  
991 p. 937-951.
- 992 37. Li, Z. and J. Bai, *Impulse discharge method to investigate the influence of gap*  
993 *width on discharge characteristics in micro-EDM*. The International Journal of  
994 Advanced Manufacturing Technology, 2017. **90**(5-8): p. 1769-1777.
- 995 38. Mayank, G., C. Fuchen, and K. Masanori, *Analysis of Reactions Determining Current*

996  
997

*Efficiency in Electrochemical Machining*. Procedia CIRP, 2018. **68**: p. 511-516.